FISEVIER

Contents lists available at ScienceDirect

# Journal of the Mechanics and Physics of Solids

journal homepage: www.elsevier.com/locate/jmps



# Lattice materials with pyramidal hierarchy: Systematic analysis and three dimensional failure mechanism maps



Qianqian Wu<sup>a,b</sup>, Ashkan Vaziri<sup>c</sup>, Mohamad Eydani Asl<sup>c</sup>, Ranajay Ghosh<sup>d</sup>, Ying Gao<sup>a,b</sup>, Xingyu Wei<sup>a,b</sup>, Li Ma<sup>a,b</sup>, Jian Xiong<sup>a,b,\*</sup>, Linzhi Wu<sup>a,e</sup>

- <sup>a</sup> Center for Composite Materials and Structures, Harbin Institute of Technology, Harbin 150001, PR China
- <sup>b</sup> National Key Laboratory of Science and Technology on Advanced Composites in Special Environments, Harbin Institute of Technology, Harbin 150080, PR China
- <sup>c</sup> Department of Mechanical and Industrial Engineering, Northeastern University, Boston, MA 02115, USA
- <sup>d</sup> Department of Mechanical and Aerospace Engineering, University of Central Florida, Orlando, FL 32816, USA
- <sup>e</sup> Key Laboratory of Advanced Ship Materials and Mechanics, College of Aerospace and Civil Engineering, Harbin Engineering University, Harbin 150001, PR China

#### ARTICLE INFO

# Article history: Received 18 October 2018 Revised 10 December 2018 Accepted 10 December 2018 Available online 12 December 2018

Keywords: Hierarchical structure Ultralight structure Lattice truss Sandwich structures Failure mechanism map

#### ABSTRACT

Sandwich core materials that offer superior mechanical properties at minimum weight are essential in designing high-performance sandwich structures. Hierarchical materials are ideal templates for this purpose. In this paper, we investigate the mechanical performance of a pyramidal-pyramidal hierarchical lattice material to highlight its potential as the core material for sandwich structures. Three-dimensional failure mechanism maps for the pyramidal-pyramidal hierarchical lattice material are developed under different loading conditions and the results are compared to finite element simulations. Next, we study the mechanical response and failure modes of a sandwich panel with self-similar pyramidal lattice core construction subjected to in-plane compression and three-point bending. The current study indicates that the pyramidal-pyramidal hierarchical configuration can improve the load bearing capacity and core buckling resistance of the sandwich structures at low density. The study provides insights into the role of structural hierarchy in tuning the mechanical response of the lattice materials and expands the application envelope of lightweight sandwich structures by effectively increasing the structural buckling resistance.

© 2018 Elsevier Ltd. All rights reserved.

# 1. Introduction

Lattice materials have attracted much interest in the past decade due to their superior mechanical properties and potential multifunctional applications (Coelho and Rodrigues, 2015; Evans, 2001; Fleck et al., 2010; Zok et al., 2016). This interest is mirrored in a recent spurt of scientific literature covering various aspects of their design, manufacturing, characterization and evaluation (For example see: Finnegan et al., 2007; Dharmasena et al., 2011; Xiong et al., 2012a,b, 2015; Cui et al., 2012; Liu et al., 2007, 2017; Han et al., 2015). One of the key areas of improvement has stemmed from using composite materials (Xiong et al., 2012a; Dong and Wadley, 2015; Liu et al., 2018) as well as novel topological designs such as structural hierarchy (Ajdari et al., 2011; Vigliotti and Pasini, 2012; Yin et al., 2013; Haghpanah et al., 2013; Fan et al., 2008; Xu et al., 2017;

E-mail address: jx@hit.edu.cn (J. Xiong).

<sup>\*</sup> Corresponding author at: Center for Composite Materials and Structures, Harbin Institute of Technology, 2 Yikuang street, Nangang, Harbin, Heilongjiang 150080, China.

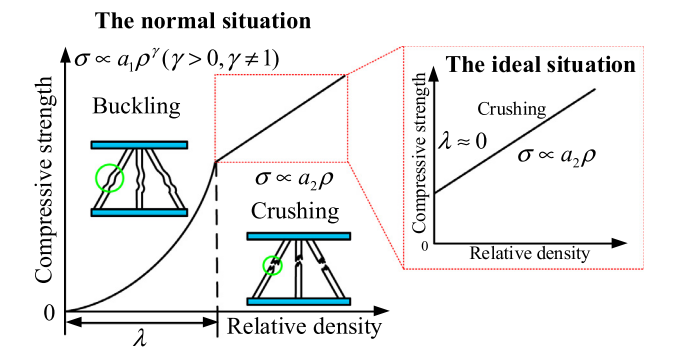


Fig. 1. An ideal ultralight weight sandwich material (with  $\lambda \approx 0$ , where  $\lambda$  is the ultralight factor) fails due to crushing of the trusses with a compressive strength that is linearly related to the material relative density. For a normal ultralight weight sandwich material with  $\lambda \geq 0$ , the truss members buckle under compression, with a buckling compressive strength that varies as a power function of the material relative density. This is followed by the crushing, where the compressive strength relates linearly to the material relative density (similar to an ideal situation).

Cote et al., 2009; Zhang et al., 2015) to achieve further weight reduction and possible multifunctional applications. On the other hand, the structured internal configuration of these lattice materials leads to complex failure modes when compared to traditional monoliths. For instance, buckling or crushing of the core member in structures with lower relative densities is regarded as a major factor that directly affects the mechanical properties of sandwich structures (Finnegan et al., 2007; Cote et al., 2009). The internal structure of these materials also leads to an inherent link between their mechanical performance such as out-of-plane compressive strength and relative density (Fan et al., 2008; Meza et al., 2015; Han et al., 2015; He et al., 2017). These lightweight lattice structures can be made even more lightweight (ultralight) by employing hierarchy on their lattice members themselves. This hierarchy leads to several interesting properties such as substantial increase in the structural mechanical performances per unit weight.

However, incorporating hierarchy by itself does not remove the failure modes due to buckling of the slender trusses. We aim our current paper towards addressing this weakness of lattice structures and aim to instill 'buckling resistance' through appropriate topological design thereby heralding an 'ideal structure'. In order to demonstrate this concept, we choose a specific *pyramidal-pyramidal* lattice truss topology, i.e. pyramidal lattice structures whose lattice members are themselves pyramidal lattice structures. We investigate these structures under out-of-plane and transverse compression, shear loading, and three-point bending. We compare our results with those of other structures studied in the literature. Closed-form expressions for the structural strength associated with different possible failure modes are also derived, and three-dimensional failure mechanism maps for sandwich panels with hierarchical lattice core construction are established. This study provides a systematic approach to evaluate the *pyramidal-pyramidal* hierarchical sandwich panels and highlights an ultralight-weight material selection for sandwich structures. This study provides a systematic investigation on the behavior and performance of ultralight-weight sandwich materials by expanding the scope of previous studies on quasi-static mechanical behaviors of sandwich structures with *corrugated-pyramidal* hierarchical lattice trusses (Wu et al., 2017).

In the next section of the paper, the concept of designing the ideal ultralight weight sandwich materials is introduced. In Section 3, the out-of-plane compressive and shear properties of the *pyramidal-pyramidal* hierarchical structure are demonstrated. The in-plane compressive and three-point bending properties of self-similar pyramidal hierarchical sandwich materials are investigated in Section 4 and 5, respectively and concluding remarks are presented in Section 6.

#### 2. Principle of ultralight weight sandwich materials

The lattice cores of sandwich structures are more susceptible to failure than the face sheets under out-of-plane compression (Finnegan et al., 2007). The buckling and crushing of truss members of the lattice core are characterized as the dominant failure modes under out-of-plane compression loading. Due to this specific feature, even for composite materials, any failure mode of lattice struts except for buckling, is considered as the crushing of lattice trusses. The distinction of these modes can be seen clearly for metallic sandwich structures where plastic yielding and plastic wrinkling of the lattice are labeled as lattice truss crushing (Feng et al., 2016). For composites, crushing mode can incorporate other damage modes. In any case, both of these broad failure modes would determine the ultimate compressive strengths of lattice core materials. This can be seen in Fig. 1 (left), which plots the compressive strength with relative density of the sandwich core. Fig. 1 shows that the compressive strength of sandwich panels under truss member buckling is proportional to a power function of the relative density which can vary according to the specific topology of the structure (Fleck et al., 2010; Fan et al., 2008; Han et al., 2015). This figure shows that the buckling led failure precedes the crushing regime and leads to much lower compressive strength in the low relative density regime. This makes ultralight material highly susceptible to failure even before the parent material experiences failure from crushing. This weakness must be eliminated for stronger and 'ideal' ultralight design. For such an ideal ultralight weight sandwich material only one failure mode would occur as shown Fig. 1 (right). When truss members fail in purely crushing mode, the compressive strength of sandwich materials is

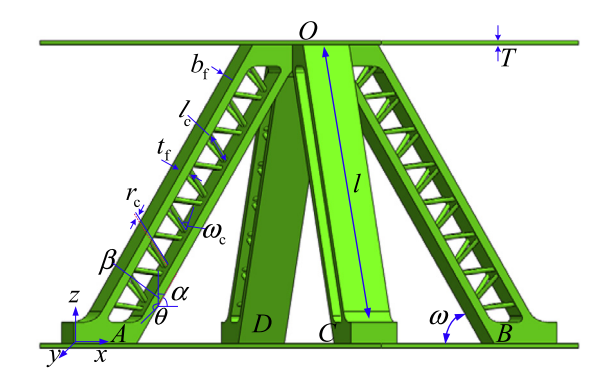


Fig. 2. The geometric dimensions and schematic of a representative unit cell of a self-similar pyramidal hierarchical sandwich structures.

linearly related to the relative density of the sandwich unit cell compared to rapid power law decrease. A non-dimensional factor  $\lambda$  is introduced as the ultralight factor which is defined as the ratio of the expression of the equivalent buckling strength to that of the equivalent crushing strength of the structural unit cell. Therefore, reduction in the ultralight factor  $\lambda$  yields the mass reduction in the sandwich structure and decreases the possibility of the buckling failure mode in the lattice trusses.

# 3. Hierarchical composite lattice truss materials under out-of-plane compression and shear loads

A typical hierarchical pyramidal truss lattice core structure has at least two different length scales for consideration, the larger 1st order length scale representing the core lattice member which connects the face sheets. The 2nd order length scale is a smaller length scale which makes up the pyramidal truss member. Note that the topological configuration of the second order (2nd order) lattice strut and that of the 1st order lattice core do not have to be identical. However, when they are similar, the structure is self-similar hierarchic (Haghpanah et al., 2013). In this paper, the topology of both orders of length scale is kept same resulting in a *pyramidal-pyramidal* cores structure. The characteristic dimensions and the schematic of the *pyramidal-pyramidal* unit cell is shown in Fig. 2. The lattice strut itself may be solid, hollow or a foam core member of various cross sections. By varying the cross section of the struts, different relative densities of the core can be obtained keeping the topology of the hierarchy constant. In this section, the out-of-plane compressive and shear properties of the *pyramidal-pyramidal* hierarchical sandwich materials will be studied. Meanwhile, the corresponding properties of pyramidal sandwich structures with various uniform cross sections of the lattice struts will be given in the Appendix for subsequent comparison. To be specific, the study of the relative density, equivalent out-of-plane stiffness and strength from Section 3.1 to 3.3 is to pave the way for the comparative studies under compression in Section 3.5. Similarly, the research on the comparison of shear properties in Section 3.9 will be based on the equivalent shear stiffness and strength from Section 3.6 to 3.7.

### 3.1. Relative density

The relative density of the core can be explicitly calculated from the geometry of the structure and cross section of the struts as shown in Fig. 2. The thickness of the face sheet is T. The length of the  $1^{\rm st}$  order pyramidal lattice truss member is I and  $\omega$  is the angle between the  $1^{\rm st}$  order pyramidal lattice truss member and the corresponding face sheet. The terms  $\alpha$ ,  $\beta$  and  $\theta$  represent the angles between the pyramidal core and the coordinate axis, respectively as shown in Fig. 2. The density of the parent material which constitutes sandwich panels is  $\rho$  and the Young modulus of parent material is E. When a foam core is considered for the strut, the density of the foam-core would be taken as  $\rho_f$  with negligible Young's modulus. The cross section area of the pyramidal unit cell A can be calculated as  $A = 2I^2 \cos^2 \omega$  and the spatial volume of the core V is equivalent to  $V = 2I^3 \cos^2 \omega \sin \omega$  (Finnegan et al., 2007).

The length of the  $2^{\rm nd}$  order lattice struts is denoted as  $l_c$  and if the cross section is circular, the radius of the strut is  $r_c$ . The angle between the  $2^{\rm nd}$  order lattice strut and the  $1^{\rm st}$  order pyramidal truss member is  $\omega_c$ . This  $1^{\rm st}$  order truss also serves as the  $2^{\rm nd}$  order 'face sheet' for the hierarchical structure as seen in Fig. 2. The thickness and width of this  $2^{\rm nd}$  order face sheet is denoted by  $t_f$  and  $b_f$  with a cross-sectional area of  $A_t$ . This  $2^{\rm nd}$  order 'sandwich structure' which is made up of  $2^{\rm nd}$  order struts and  $1^{\rm st}$  order truss members as face sheet is characterized by a cross-sectional area  $A_c$ . The equivalent density of this  $2^{\rm nd}$  order pyramidal core sandwich structure  $\rho_{ce}$  is

$$\rho_{ce} = \frac{\left(\sqrt{2}A_t \cos \omega + 2A_c\right)\rho}{l_c^2 \cos^2 \omega \sin \omega} \tag{1}$$

This can be used to compute the density and relative density of the overall (1<sup>st</sup> order) hierarchical pyramidal structure as well. If the cross-sectional area of the 1<sup>st</sup> order pyramidal lattice strut is denoted as  $A_a$ , the mass of the 1<sup>st</sup> order lattice

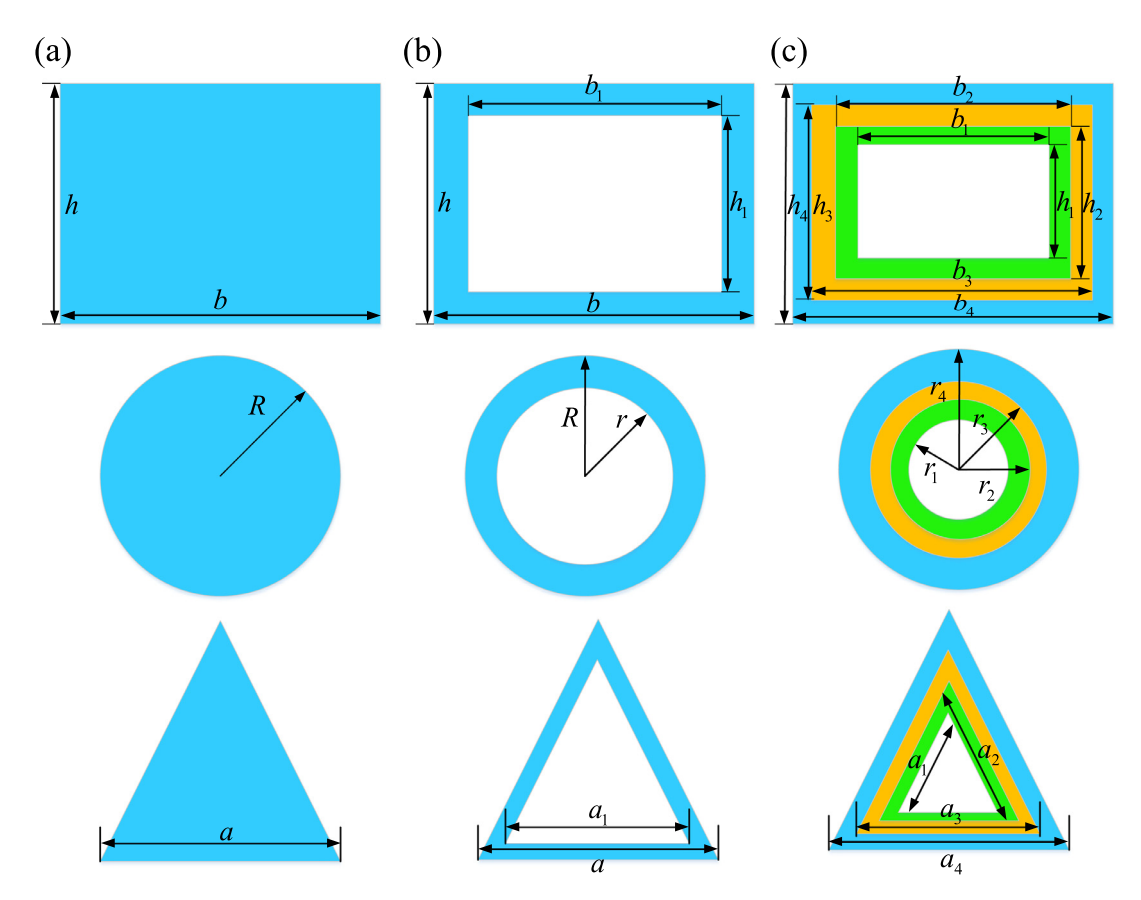


Fig. 3. Cross-section of different lattice struts with various configurations: (a) solid lattice truss, (b) hollow lattice truss, and (c) foam-core lattice truss.

core would be  $M = 4lA_a\rho_{ce}$ . The equivalent density and relative density of the hierarchical structure can then be calculated using Eqs. (2) and (3).

$$\rho_e = \frac{2A_a \rho_{ce}}{l^2 \cos^2 \omega \sin \omega} \tag{2}$$

$$\bar{\rho} = \frac{A_{\rm a} \left(2\sqrt{2}A_{\rm t}\cos\omega + 4A_{\rm c}\right)}{l^2 l_{\rm c}^2 \cos^4\omega \sin^2\omega} \tag{3}$$

This expression can be specialized for different strut cross sections of the  $2^{nd}$  order structure, shown in Fig. 3 (see Appendix 1 for these expressions).

# 3.2. The equivalent out-of-plane compressive stiffness

The pyramidal unit cells are assumed to have a small displacement  $\delta$  along the load direction under out-of-plane compression. The external force of each pyramidal lattice truss F can then be written as (see Section 3.1 of the Appendix 3 for details):

$$F = \frac{(EA)_e l^2 \sin^2 \omega + 12(EI)_e \cos^2 \omega}{l^3} \delta$$
 (4)

where  $(EA)_e$  and  $(EI)_e$  denote the equivalent compressive stiffness and the equivalent flexural rigidity of the lattice core, respectively. The equivalent stress of the pyramidal unit cell can be expressed as  $\overline{\sigma}=4F/A$ . Substituting Eq. (4) and the area of pyramidal unit cell into this expression, the equivalent stress of the pyramidal sandwich panels can be calculated as:

$$\bar{\sigma} = \frac{2(EA)_e l^2 \sin^2 \omega + 24(EI)_e \cos^2 \omega}{l^5 \cos^2 \omega} \delta \tag{5}$$

The non-dimensional parameter  $\xi_{\omega}$  is defined as:

$$\xi_{\omega} = \frac{(EA)_e l^2 \sin^2 \omega + 12(EI)_e \cos^2 \omega}{(EA)_e l^2 \sin \omega} \tag{6}$$

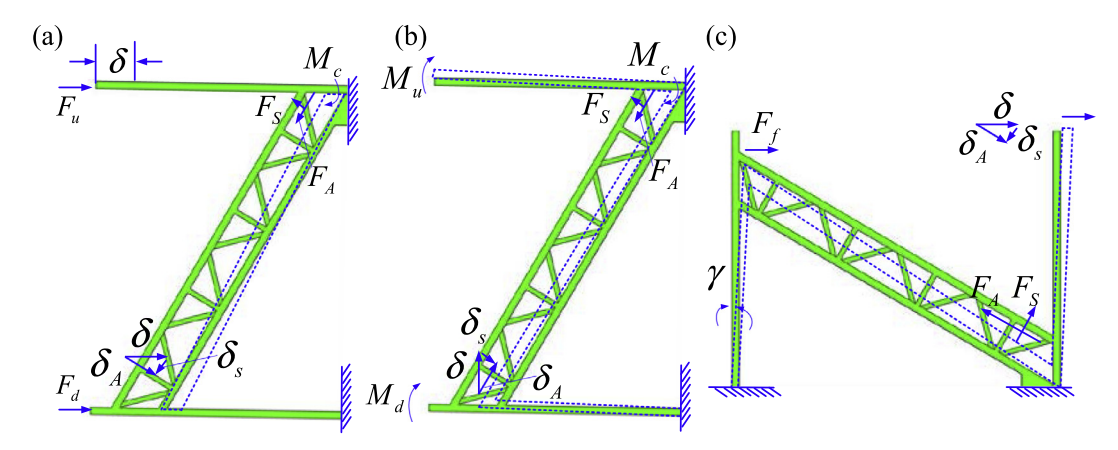


Fig. 4. The free-body-diagram of truss unit cells under (a) in-plane compression, (b) bending moment, and (c) shear load.

The equivalent stress can be further simplified into:

$$\bar{\sigma} = \frac{2\xi_{\omega}(EA)_e \sin \omega}{\beta \cos^2 \omega} \delta \tag{7}$$

The equivalent strain of the unit cell along the z-axis direction is then given by  $\overline{\varepsilon} = \delta/l \sin \omega$ . The out-of-plane compressive stiffness  $\overline{E}$  is  $\overline{E} = \overline{\sigma}/\overline{\varepsilon}$ . Substituting Eq. (7) into the expression of the compressive stiffness, the corresponding expression becomes:

$$\bar{E} = \frac{2\xi_{\omega}(EA)_{e}\sin^{2}\omega}{l^{2}\cos^{2}\omega}$$
(8)

With the equivalent compressive stiffness  $(EA)_e$  and the non-dimensional parameter  $\xi_\omega$  of various types of pyramidal lattice trusses, the equivalent out-of-plane compressive stiffness of different pyramidal sandwich panels can be obtained using Eq. (8). Meanwhile, the effects of the cross-sectional characteristics of the  $2^{\rm nd}$  order struts on the compressive stiffness  $\overline{E}$  of the sandwich structure and a non-dimensional parameter  $\xi_\omega$  can also be studied analytically (see Appendix 2 for details).

The equivalent compressive stiffness of the hierarchical sandwich structure can be found using the principle of virtual work. A lateral compressive load F is applied to the 1<sup>st</sup> order unit cell of the *pyramidal-pyramidal* structure, with a corresponding displacement  $\delta$  as shown in Fig. 4(a). Using virtual work calculation (shown in Section 3.2 of the Appendix 3), the relationship between F and  $\delta$  can be obtained as:

$$F = \frac{2(EA)_f}{l\cos\beta}\delta + \frac{2(EA)_e l^2 \cos^2\beta + 24(EI)_e \sin^2\beta}{l^3}\delta$$
(9)

where the compressive stiffness and the flexural rigidity of the  $2^{\rm nd}$  order pyramidal truss member with circular section are  $(EA)_c = E\pi r_c^2$  and  $(EI)_c = E\pi r_c^4/4$  respectively and the compressive stiffness of the  $2^{\rm nd}$  order face sheet is  $(EA)_f = Eb_c t_f$ . On the other hand, the equivalent strain of the hierarchical sandwich structure is

$$\bar{\varepsilon} = \frac{\delta}{2l_c \cos \beta} \tag{10}$$

The equivalent compressive stiffness of pyramidal-pyramidal lattice truss structures  $(EA)_e = F/\bar{\epsilon}$  can be expressed as:

$$(EA)_{e} = 2Eb_{c}t_{f} + \frac{6E\pi r_{c}^{4}\sin^{2}\beta\cos\beta}{l_{c}^{2}} + 2E\pi r_{c}^{2}\cos^{3}\beta$$
(11)

Similarly, virtual work can also be used to obtain the equivalent flexural rigidity of the unit cell by applying a bending moment M to the lateral surface of the 1<sup>st</sup> order unit cell of the structure. Through the structural symmetry of the structure shown in Fig. 4(b), the equivalent flexural rigidity of this unit cell is found to be (see Section 3.2 of the Appendix 3 for details)

$$(EI)_{e} = 2(EI)_{m} + \left[ f_{3}(\beta, \theta) E \pi r_{c}^{4} + f_{4}(\beta, \theta) l_{c}^{2} E r_{c}^{2} \right]$$
(12)

where  $f_3(\beta, \theta)$  and  $f_4(\beta, \theta)$  are defined as  $\cos \beta - \frac{3}{2} \cos^2 \beta \sin \theta + \frac{3}{4} \cos^3 \beta \sin^2 \theta$  and  $\frac{1}{4} \cos^3 \beta \cos^2 \theta$ , respectively.

These stiffness and rigidities can be substituted in Eqs. (6) and (8) to obtain the non-dimensional strength and stiffness of the hierarchical sandwich structure (1<sup>st</sup> order).

# 3.3. The equivalent out-of-plane compressive strength

The equivalent compressive stress of the pyramidal cell has been listed in Eq. (7), the relationship among the axial force of struts, the inherent strength of the materials and the equivalent compressive stress of the structures will be established in this section, and then the corresponding equivalent strength of the pyramidal unit cell associated with various truss member's failure modes is derived. The out-of-plane compressive force F is assumed to be applied in the normal direction to the sandwich panels. The relationship between the axial force  $F_A$ , the shear force  $F_S$  and the bending moment M of a single truss and the resultant force F of the 1<sup>st</sup> order pyramidal unit cell can be given as (see Section 3.2.2 of the Appendix 3 for details):

$$F = 4\xi_{\omega}F_{A} \tag{13}$$

$$F_{\rm S} = \frac{12(EI)_e \cos \omega}{(EA)_e l^2 \sin \omega} F_A \tag{14}$$

$$M = \frac{6(EI)_e \cos \omega}{(EA)_e I \sin \omega} F_A \tag{15}$$

Eqs. (14) and (15) denote the ratio of the shear force and the bending moment to the axial force which can be sufficiently small assuming that the pyramidal truss members are relatively slender. Therefore, the axial force can be regard as a dominant destructive force which induces the failure of the pyramidal lattice truss under out-of-plane compressive loads. If the magnitude of the external force is F, the equivalent out-of-plane compressive strength of the pyramidal unit cell  $\overline{\sigma}$  can be expressed as:

$$\bar{\sigma} = \frac{F}{2l^2 \cos^2 \omega} \tag{16}$$

In this section, the hierarchical *pyramidal–pyramidal* lattice truss sandwich panel with four different modes of failure under out-of-plane compressive loads is considered. The failure modes include face sheet wrinkling (FW) of the 2<sup>nd</sup> order lattice truss, face sheet crushing (FC) of the 2<sup>nd</sup> order lattice truss (which is same as crushing of 1<sup>st</sup> order truss member), core member Euler buckling (CE) of the 2<sup>nd</sup> order lattice truss and Euler buckling of the 1<sup>st</sup> order pyramidal truss. The corresponding schematic of failure modes of hierarchical pyramidal sandwich unit cell is shown in Fig. 5. In the following, each failure mode is described.

Here, it's imperative to describe the derivation of various failure modes accordingly. The critical load F of the  $2^{\rm nd}$  order face sheet or hierarchical lattice truss can be primarily obtained by means of the elementary mechanics formulas. In order to obtain the instability envelopes, the externally applied force on the face sheets ( $1^{\rm st}$  order lengths scale) is transferred to the local axial force of the strut ( $2^{\rm nd}$  order length scale) using relationships derived earlier and the equations tabulated in Table 2. The corresponding equivalent compressive strength  $\sigma$  can be further derived by substituting the axial force into Eqs. (13) and (16). Table 2 lists the equivalent compressive strength of each failure mode. In Table 2, the abbreviation ECS denotes the equivalent compressive strength of the hierarchical sandwich structure. The non-dimensional parameters  $\xi_p$  and  $\xi_\omega$  are in Eq. (A-13) and Table A-3, respectively. For core member buckling of the  $2^{\rm nd}$  order lattice truss, the dimensionless parameter  $\lambda_p$  is

$$\lambda_p = \cos \beta + \frac{3r_c^2 \sin^2 \beta}{l_c^2 \cos \beta} + \frac{4l_c t_f}{\cos \beta \pi r_c^2} \tag{17}$$

The equivalent out-of-plane compressive strength of the pyramidal sandwich structures with the uniform cross section lattice struts has been described in Section 3.2.2 of the Appendix 3.

# 3.4. Numerical simulation and failure mechanism map under compressive loads

In this section, numerical simulations are conducted to validate the accuracy of the analytical derivation and investigate the mechanical response of the *pyramidal-pyramidal* hierarchical sandwich structure under compressive loads. A commercial finite element (FE) package ABAQUS (Dassault Systemes) was used for all numerical simulations. Table A-1 lists the geometrical characteristics of different sample geometries analyzed computationally for compressive stiffness and compressive strength calculations. In this study, the mechanical properties of carbon fiber reinforced epoxy composites are used for establishing the material model in the numerical analysis. The elastic modulus and compressive strength of the parent material are 100 GPa and 800 MPa, respectively, and Poisson's ratio is 0.3. In the simulation, rigid face sheets were tied to the lattice core structure at the interface nodes. While the bottom face sheet was fixed, a compressive displacement was then applied to the top face sheet to simulate core crushing. The models were meshed using three-dimensional 8-node linear brick elements with reduced integration (i.e., C3D8R element in ABAQUS), and a mesh sensitivity analysis was performed to guarantee that the results were not mesh-dependent. Static-general solver of ABAQUS was used to simulate the response of the structures under compressive loads. Moreover, in the numerical model, two pyramidal unit cells were used along the width of the first order pyramidal core struts.

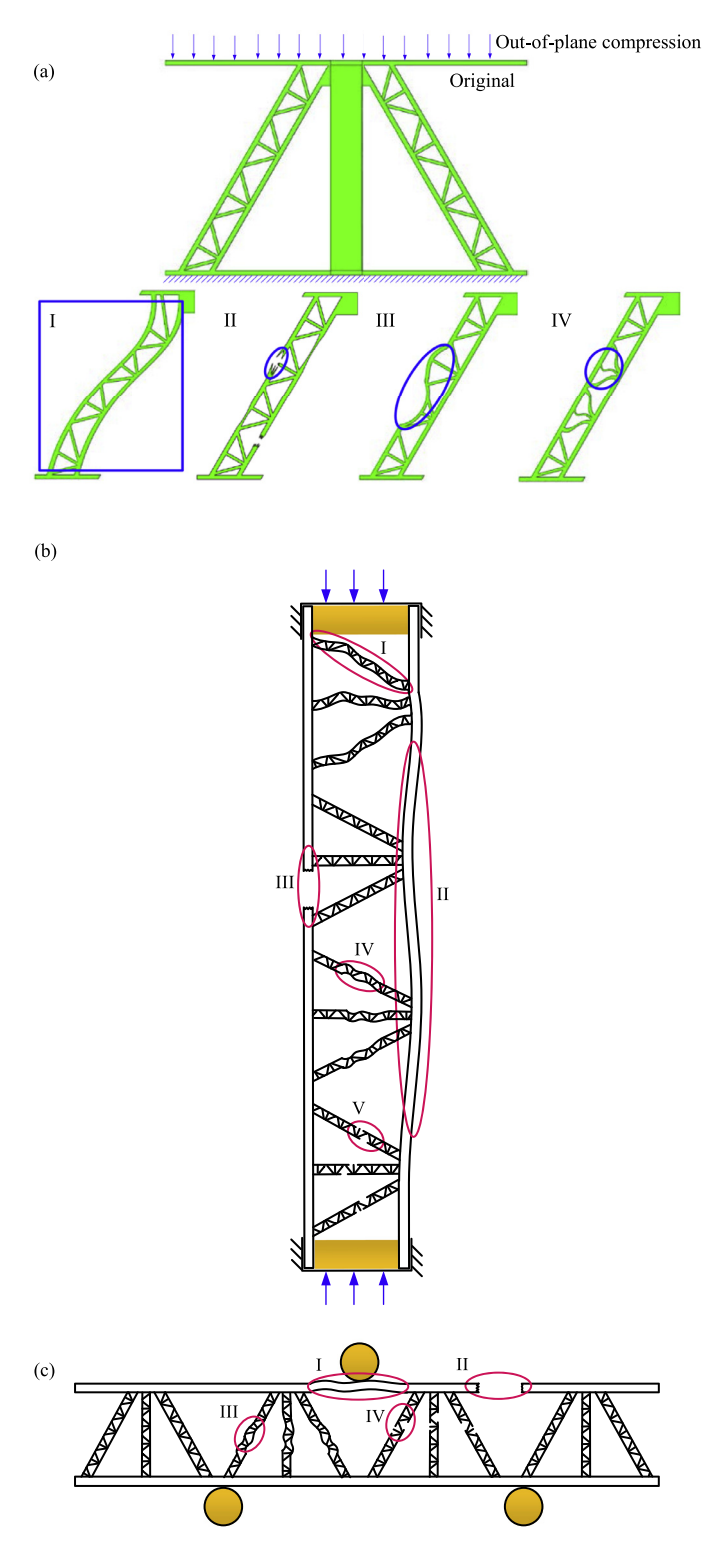


**Fig. 5.** (a) Failure modes of the *pyramidal-pyramidal* 2<sup>nd</sup> order lattice truss under out-of-plane compression: (I) Macro Euler buckling of the 1<sup>st</sup> order pyramidal truss, (II) Face sheet crushing (FC) of the 2<sup>nd</sup> order lattice truss, (III) Face sheet wrinkling (FW) of the 2<sup>nd</sup> order lattice truss, (IV) Core member buckling (CE) of the 2<sup>nd</sup> order lattice truss. (b) Failure modes in the *pyramidal-pyramidal* columns subjected to in-plane compression load. (I) Macro Euler buckling of the 1<sup>st</sup> order pyramidal truss, (II) FW of the 1<sup>st</sup> order pyramidal truss, (IV) FW of the 2<sup>nd</sup> order lattice truss. (c) The schematic diagram of failure modes of hierarchical face sheet under three-point bending load: (I) FW of the 1<sup>st</sup> order pyramidal truss, (III) FC of the 1<sup>st</sup> order pyramidal truss, (IV) FC of the 2<sup>nd</sup> order lattice truss.

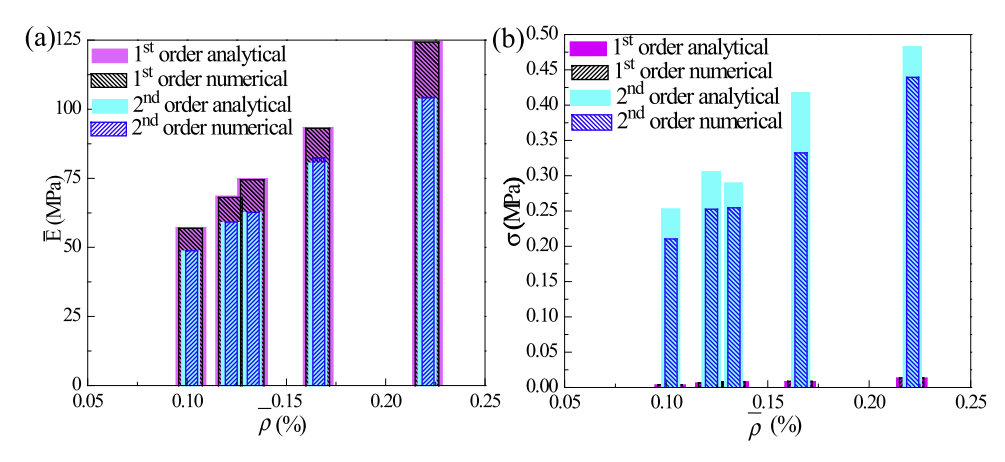


**Fig. 6.** Comparisons of the materials properties between the 2<sup>nd</sup> order lattice truss and the 1<sup>st</sup> order pyramidal truss at different relative densities (the number of unit cells is equal to 51): (a) Compressive stiffness, and (b) Compressive strength.

Numerical simulations showed that the number of the 2<sup>nd</sup> order pyramidal unit cells has a significant effect on the error between the theoretical and numerical results. The error decreases with an increase in the number of the 2<sup>nd</sup> order unit cells. Meanwhile, some existing studies (Cote et al., 2007; Li et al., 2011; Biagi and Bart-Smith, 2012) have validated their relationship. It is worth noting that the macroscopic elastic buckling failure mode of the member is also usually predicted by the traditional Euler's buckling formula in these studies. Here, taking the pyramidal-pyramidal hierarchical structure with 51 secondary unit cells under various relative densities (0.102%-0.221%) as an example, the difference between theoretical and numerical results will be compared. In Fig. 6, the analytical and numerical results of the compressive stiffness or compressive strengths are compared based on several common relative densities. In this histogram the width of each bar graph was changed in order to visually distinguish them. Fig. 6(a) lists the out-of-plane compressive stiffness of the 1st and 2nd order lattice truss under various relative densities (0.102%-0.221%). Excellent agreement is observed between the analytical and FE results for the compressive stiffness of the 1st and 2nd order lattice truss. The results presented in Fig. 6(a) show that the out-of-plane compressive stiffness of the pyramidal-pyramidal 2<sup>nd</sup> order lattice truss is slightly lower than its 1<sup>st</sup> order counterpart. Our FE simulations also show that in contrast to the 1st order pyramidal truss in which the deformation is uniformly distributed between all truss members, for the pyramidal-pyramidal 2<sup>nd</sup> order lattice truss, the majority of the load is carried by the 2<sup>nd</sup> order face sheets, and the 2<sup>nd</sup> order truss members make relatively small contribution to the overall stiffness of the structure. The out-of-plane compressive strengths of the 1st and 2nd order lattice truss as a function of the relative density (0.102%-0.221%) are given in Fig. 6(b). This figure shows that for sandwich panels with the 1<sup>st</sup> order lattice truss, the error between theoretical and numerical results is less than 5%. The corresponding magnitude of the equivalent compressive strength is summarized in Table 6. The numerical results agree well with the theoretical results for both the 1<sup>st</sup> order and hierarchical pyramidal sandwich structures.

According to the compressive strength prediction formula of hierarchical pyramidal sandwich panels under various failure modes, a three-dimensional failure mechanism map of pyramidal hierarchical sandwich panels under out-of-plane compression can be generated, Fig. 7(a). The nature of failure which is primarily due to structural instability allows this phase diagram to be mapped using normalized geometric parameters  $r_c/l_c$ ,  $l_c/l_f$  and  $t_f/l_c$  ( $\omega=\omega_1=45^\circ$  for this study). The 3D failure map and the 2D failure mechanism diagram of the three perspectives (x-y plane, x-z plane and y-z plane, namely,  $t_f/l_c = r_c/l_c = l_c/l = 0.05$ ) are given at the same time in order to improve the readability of the results. The 2D failure map when the parameter  $t_f|l_c$  is 0.01, 0.03, 0.04 and 0.1 is also given. The relationship between the failure modes of the hierarchical structure and geometric parameters of the structure is described as follows. When the parameter  $t_f/l_c$  increases from 0.01 to 0.03, the area corresponding to the Euler buckling failure mode of the 2<sup>nd</sup> order and 1<sup>st</sup> order pyramidal struts increases and the area corresponding to the  $2^{nd}$  order face sheet wrinkling decreases. When the parameter  $t_f/l_c$  increases to 0.04, the 2<sup>nd</sup> order face sheet wrinkling disappears and the 2<sup>nd</sup> order face sheet crushing appears. When the parameter increases to 0.1, the area of several failure modes in the failure mechanism maps remains substantially constant. Compared to the traditional planar failure mechanism map, three-dimensional failure mechanism diagram can accurately visualize the location of the failure mode with all three sets of geometric parameters in one single plot. This also allows for easy observation of trends in all three variables since 3D failure mechanism map can be used to visualize 2D failure mechanism maps from various perspectives simultaneously. At the 2<sup>nd</sup> order scale, face sheet wrinkling and face sheet crushing failure modes are considered as two dominant failure modes. The core member buckling of the 2<sup>nd</sup> order lattice truss can be only observed when the normalized parameter  $r_c/l_c$  is very small. The core member buckling of the 1<sup>st</sup> order lattice truss can also be observed when the parameter  $l_c/l$  is very small. These failure mechanism maps can be used to design hierarchical lattice core materials which avoid lying inside undesirable failure regions. To ascertain the feasibility of fabricating pyramidal-pyramidal hierarchical sandwich structure, this could be especially useful for additive manufacturing based design where substantially

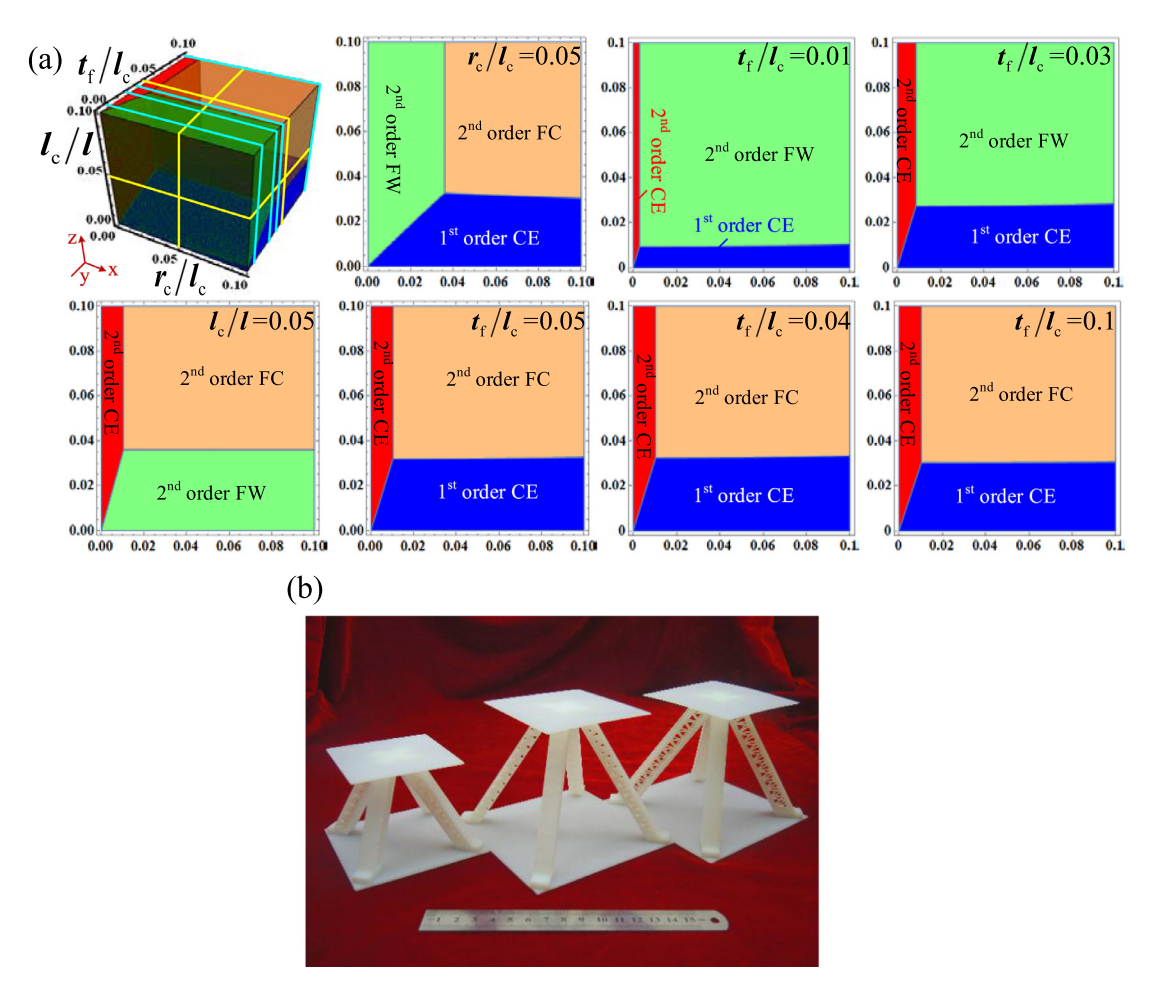


**Fig. 7.** (a) Failure mechanism maps of the 2<sup>nd</sup> order lattice truss under out-of-plane compression where FW denotes face sheet wrinkling, FC denotes face sheet crushing and CE denotes core member buckling. (b) Samples of hierarchical *pyramidal-pyramidal* sandwich structures manufactured using 3D printing technology.

complicated geometries may be manufactured. We show several unit cells of different sizes which are based on this method of design in Fig. 7(b).

### 3.5. Comparative out-of-plane compressive properties

This section compares the out-of-plane compressive properties of regular pyramidal and hierarchical *pyramidal-pyramidal* sandwich structures of same relative density and parent material. We also compare the compressive strength of the *pyramidal-pyramidal* hierarchical sandwich panels to that of the previous studies in the literature demonstrating the mechanical performance of the ideal ultralight weight sandwich materials. Such an analysis facilitates and expedites the selection of sandwich panels with desired compression performance. The compression behavior of these sandwich structures is described in detail as follows.

### 3.5.1. Stiffness of pyramidal-pyramidal hierarchical lattice structures

To compare the out-of-plane compressive stiffness of hierarchical pyramidal sandwich panels with uniform cross-section lattice truss, the out-of-plane compressive stiffness of *pyramidal-pyramidal* hierarchical structures is expressed as a function of relative density. In addition, when comparing the out-of-plane stiffness of two structures we need to ensure that the structural unit cells maintain the same relative density. Due to the complicated structure of the  $2^{\rm nd}$  order pyramidal lattice truss leading to complex geometric quantities, it becomes necessary to set the proportional relationship between the geometric parameters. We set  $t_f = ml_c$  and  $r_c = m^2 l_c$  and m is a dimensionless proportionality coefficient. Substituting Eqs. (3) and (11) into Eq. (8), the equivalent out-of-plane compressive stiffness of pyramidal hierarchical structures is

$$\bar{E} = \frac{\sqrt{2}\xi_{\omega}Ef_{p}(m)}{4}\bar{\rho} \tag{18}$$

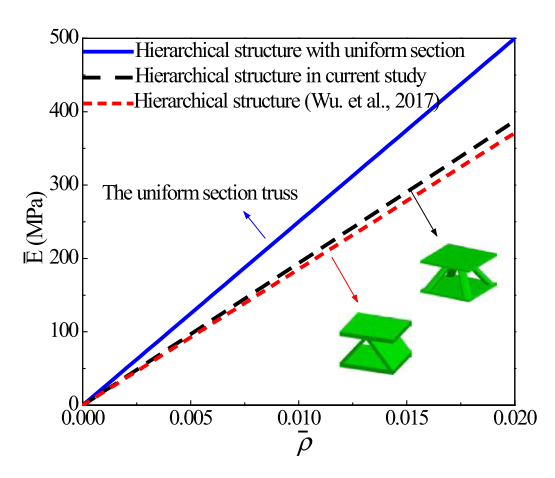


Fig. 8. Comparison of out-of-plane compressive stiffness of hierarchical structures with corrugated, pyramidal truss sandwich struts and uniform sectional foam-core struts.

$$f_p(m) = \frac{8 + \pi m^3 + 9\pi m^7}{8(1 + 2\sqrt{2}m)(1 + 2\pi m^3)}$$
(19)

where the dimensionless parameter value  $\xi_{\omega}$  in Eq. (18) is similar to that of the uniform cross-section core rod, namely,  $\xi_{\omega} \approx \sin \omega$ . The structural function  $f_p(m)$  indicates the proportion of stiffness change after changing from uniform cross-section lattice trusses to the pyramidal hierarchical truss members.

The equivalent out-of-plane compressive stiffness of the uniform cross-section lattice trusses can be expressed as a function of relative density using the expressions given in Section 3.3.1 of the Appendix 3. The trends of the equivalent compressive stiffness versus relative density for three hierarchical structures with m = 0.1 is shown in Fig. 8. The uniform cross-sectional hierarchical lattice structure has superior equivalent compressive stiffness, and the equivalent compressive stiffness of the *corrugated-pyramidal* hierarchical structure (Wu et al., 2017) is slightly inferior to that of the self-similar pyramidal structure in current study. As shown in Fig. 8, the compressive stiffness of *pyramidal-pyramidal* hierarchical structures and that of *corrugated-pyramidal* hierarchical structures decreases by about 22.5% and 25.8%, respectively. This is because each part of truss members in hierarchical sandwich structures with uniform cross section is subjected to the same out-of-plane compressive load. However, for the *pyramidal-pyramidal* hierarchical lattice truss, the main external load is imposed on the  $2^{nd}$  order face sheets. In addition, the material between the  $2^{nd}$  order face sheets makes little contribution for the structural compressive stiffness but increases the weight of the structure. Therefore, when compared to the  $1^{st}$  order pyramidal structure, the compressive stiffness of *pyramidal-pyramidal* hierarchical structure decreases under the same weight of structure.

#### 3.5.2. Strength of pyramidal-pyramidal hierarchical lattice structures

To compare the hierarchical panels with uniform cross-sectional truss members, the compressive strength of *pyramidal-pyramidal* hierarchical structures should be expressed as a function of relative density which can be compared against the 1<sup>st</sup> order pyramidal sandwich structures described in the previous section. Also, the geometric parameters of the hierarchical structure should conform to the previous framework:  $t_f = ml_c$  and  $r_c = m^2 l_c$ . Here, the equivalent compressive strength of the structure under these two failure modes (2<sup>nd</sup> order FC and 1<sup>st</sup> order CE) is the same with that in Table 2. However, the equivalent compressive strength in this section needs to be expressed as a function of relative density. When the 2<sup>nd</sup> order face sheet crushing failure mode occurs, the equivalent compressive strength of the structure is

$$\bar{\sigma} = \xi_{\omega} (1 + \xi_p) \sigma_f f_{fp}(m) \bar{\rho} \tag{20}$$

where the parameter  $f_{fp}(m)$  in Eq. (20) can be expressed as a function of m as  $f_{fp}(m) = 1/(\sqrt{2} + 4m)(1 + 2\pi m^3)$ .

When the overall Euler buckling of the 1<sup>st</sup> order truss members occurs, the equivalent compressive strength of the structure can be obtained by substituting the relative density and the equivalent compressive stiffness in Eqs. (3) and (12) into the equivalent compressive strength under the 1<sup>st</sup> order CE failure mode in Table 2. This leads to

$$\bar{\sigma} = \xi_{\omega} \pi^2 E f_{pp}(m) \bar{\rho}^2 \tag{21}$$

where

$$f_{bp}(m) = \frac{\frac{35 - 12\sqrt{2}}{64}\pi m^7 + \frac{1}{64}m^3 + \frac{2}{3}m^2 + \frac{\sqrt{2}}{2}m + \frac{1}{4}}{4m(\sqrt{2} + 4m)^2(1 + 2\pi m^3)^2}$$
(22)

The relationship between the equivalent out-of-plane compressive strength and relative density of the uniform cross-section lattice trusses and the nature of the curves in Fig. 9(a)-(d) have been fully described in Section 3.3.2 of the

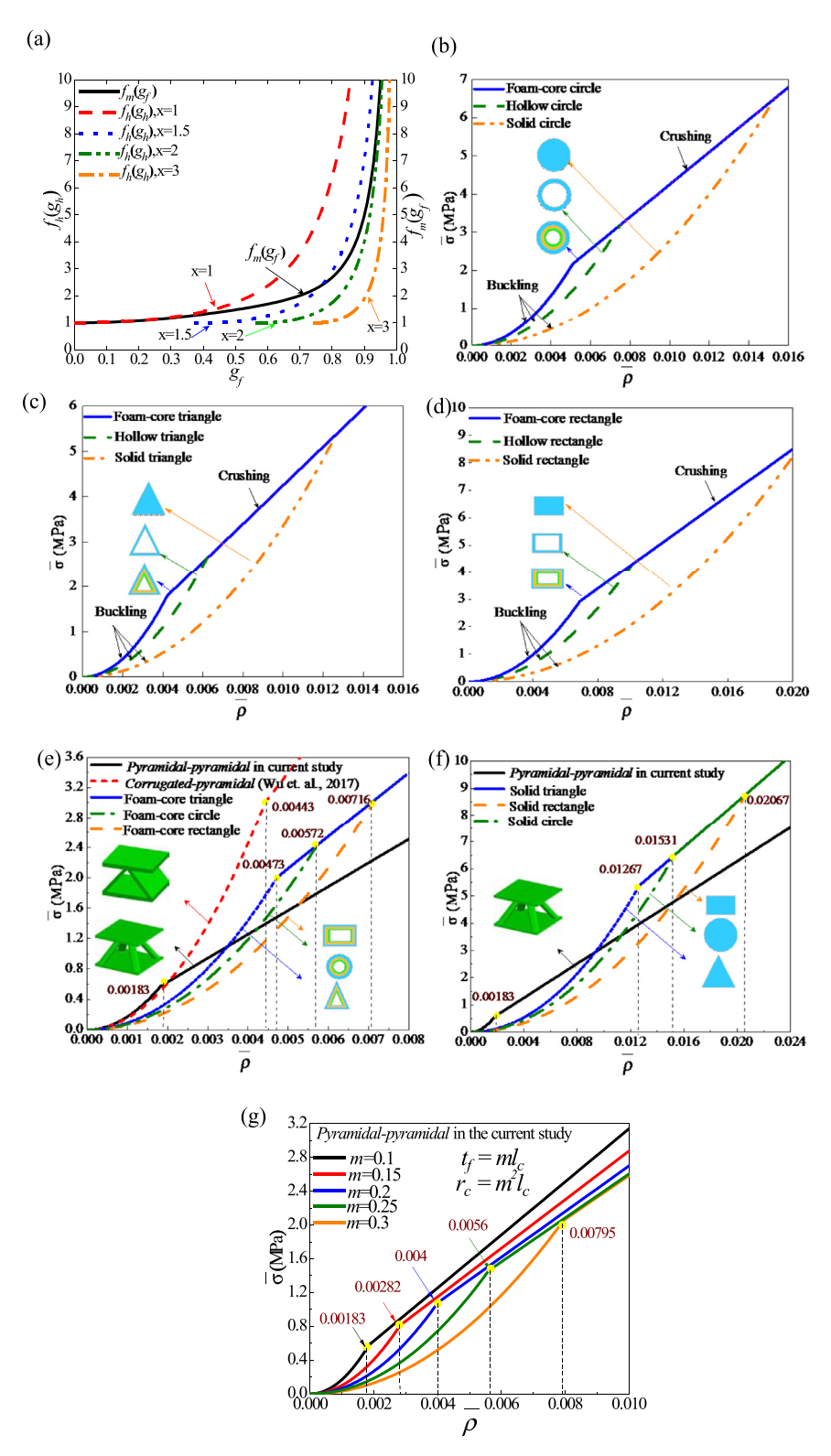


**Fig. 9.** The aggregate out-of-plane compressive properties of hierarchical sandwich structures: (a) the variation of structural functions under different conditions, (b) compressive strength of various circular cross-sections, (c) compressive strength of various triangular cross-sections, (d) compressive strength of various rectangular cross-sections, (e) the equivalent out-of-plane compressive strength of hierarchical sandwich structures with all cross-sections in the present paper, (f) the comparison of the anti-buckling capacity between the *pyramidal-pyramidal* hierarchical and the first order uniform cross-sectional lattice trusses, (g) the relationship between the proportional coefficient *m* and the structural equivalent compressive strength in the *pyramidal-pyramidal* hierarchical sandwich structure.

Appendix 3. The strength of foam hollow sandwich struts is the largest for that of rectangular, circular and triangle struts (see Fig. 9(b)-(d) for details) and their strength will be compared with that of hierarchical structures with corrugated (Wu et al., 2017) and pyramidal truss sandwich strut. The equivalent compressive strength versus relative density is shown in Fig. 9(e) for m = 0.1. Fig. 9(e) also shows the sandwich structures with uniform cross-sectional truss members (rectangular, circular and triangular) with the superior anti-buckling feature to other cross-sectional configurations of struts with the same shape. The ability of pyramidal-pyramidal hierarchical unit cells to resist buckling is distinctly better than that of the hierarchical sandwich structures with uniform cross-sections as shown in Fig. 9(e). The 2<sup>nd</sup> order hierarchical structure in this study shows distinctly better strength. This is because the intricate hierarchical structure can distribute the load more efficiently over the material points. For the self-similar pyramidal and corrugated-pyramidal hierarchical structures, the only difference in the expression for the equivalent compressive strength of the two hierarchical structures under these two failure modes is that some parameters in these equations are related to the internal geometric features of the hierarchical structures. In fact, the 2<sup>nd</sup> order corrugated and pyramidal lattice trusses mainly increase the flexural rigidity of the 1<sup>st</sup> order struts via discretely placed materials. Therefore, the thickness of the 2<sup>nd</sup> order face sheets will be small relative to the distance between the two face sheets. Here, the parameter m denotes the proportional relationship between the  $2^{nd}$  order face sheets and the spacing of the face sheets. In Eq. (20),  $\xi_{\omega} \approx \sin \omega$  and the parameter  $\xi_{D}$  is much smaller than 1. The compressive strength of the parent material  $\sigma_f$  is equal to 800 MPa. The difference in the equivalent compressive strength of two hierarchical structures under these two failure modes is only reflected on the parameters  $f_{fp}$  and  $f_{hp}$ . Under the ultra-low densities, the intersections of the pyramidal-pyramidal and corrugated-pyramidal hierarchical lattice structures are 0.00183 and 0.00443, respectively. This structure shows even better characteristics than the corrugated-pyramidal hierarchical sandwich panels because the core materials of the pyramidal truss cores are lighter than the corrugated core with a similar load-carrying ability. Fig. 9(f), which shows the comparison of the anti-buckling capacity between the pyramidal-pyramidal hierarchical and the first order uniform cross-sectional lattice trusses further illustrates the benefits of hierarchy. The relative density corresponding to the intersection of the two failure modes in the hierarchical structure is more than 6 times smaller than that of the first order uniform cross-sectional lattice trusses. In other words, the pyramidal-pyramidal hierarchical sandwich structure has stronger buckling resistance than the first order pyramidal structure with various cross-sectional shapes. To highlight the key distinctions of how geometry influences each of the failure mechanisms in the pyramidal-pyramidal hierarchical structure, the relationship between the proportional coefficient m and the equivalent out-of-plane compressive strength of the self-similar pyramidal hierarchical structure is shown in Fig. 9(g). Here, the parameter m establishes the relationship among the  $2^{nd}$  order core radius  $r_c$ , the length of the  $2^{nd}$  order strut  $l_c$  and the thickness of the  $2^{nd}$  order face sheet  $t_c$ . As the proportional coefficient m increases, the intersection of the two failure modes (core member buckling and crushing) in the pyramidal-pyramidal hierarchical structure appears later. In other words, assuming that the thickness of the 2<sup>nd</sup> order face sheet remains unchanged, the length of the 2<sup>nd</sup> order struts is reduced and the 2<sup>nd</sup> order core radius is increased, which leads to weakening of the anti-buckling capacity of the self-similar pyramidal hierarchical lattice trusses. Therefore, the three geometric parameters described earlier have a significant influence on the buckling resistance of the hierarchical structure studied in this paper.

# 3.5.3. Out-of-plane compressive strength of sandwich structures previously studied in the literature

Using the proposed concept of the ideal ultralight weight sandwich materials in Section 2, the equivalent compressive strength of different topological configurations from literature is compared to the hierarchical pyramidal-pyramidal lattice sandwich structures as a function of density of structural parent materials as shown in Fig. 10. Typical materials used in literature are Al and Carbon fiber (Fan et al., 2008; Fan and Fang, 2009). Here, the elastic modulus and compressive strength of aluminum alloy are 70 GPa and 110 MPa, respectively. The compressive stiffness and compressive strength of aluminum foam are 2 GPa and 5 MPa. To show the advantage of hierarchical sandwich structure in an ultra-low density region, the density of sandwich structure is fixed in the range of 0 to 1 g/cm<sup>3</sup>. Here, in Fig. 10(a), the abscissa uses logarithmic coordinates and the ordinate uses linear coordinates. To compare the out-of-plane compression performance between the hierarchical structure and the first order structure, we investigated different topological configurations, an isogrid, pyramid, honeycomb and foam. The compressive strength of the first order and hierarchical structures corresponding to various configurations varies with density as shown in Fig. 10(a), and the schematic diagram of four topological configurations is given in Fig. 10(b). By comparing the structure of any configuration in Fig. 10(a), the compression performance of the hierarchical structure is superior to the first order structure under the same density. In addition, for pyramidal-pyramidal hierarchical sandwich structures, the material properties of carbon fiber reinforced composite and aluminium alloy are seperately assigned to investigate the effect of the material properties on the structural response. The material properties are shown to only have an effect on the buckling strength of structures with no significant effect on the ultralight factor  $\lambda$ .

Comparing the four types of the hierarchical sandwich structures in Fig. 10(a) suggests that the *pyramidal–pyramidal* hierarchical sandwich structure buckle primarily at lower densities. As a result, a density of 0.01 g/cm<sup>3</sup> leads to an equivalent compressive strength of about 1.1 MPa for the aluminum *pyramidal–pyramidal* hierarchical sandwich structures. However, for the hierarchical honeycomb and hierarchical isogrid, their equivalent compressive strength is far less than that of the former with the same density. Similarly, the comparison between the aluminum 1<sup>st</sup> order pyramidal and hierarchical *pyramidal–pyramidal-pyramidal* lattice trusses suggest that the anti-buckling and anti-crushing abilities of the latter are superior to those of the former with the same density. The equivalent compressive strength of *pyramidal–pyramidal* hierarchical sandwich structure is greater than that of the 1<sup>st</sup> order pyramidal structure under the same density as well. As shown in Fig. 10(a), the equivalent

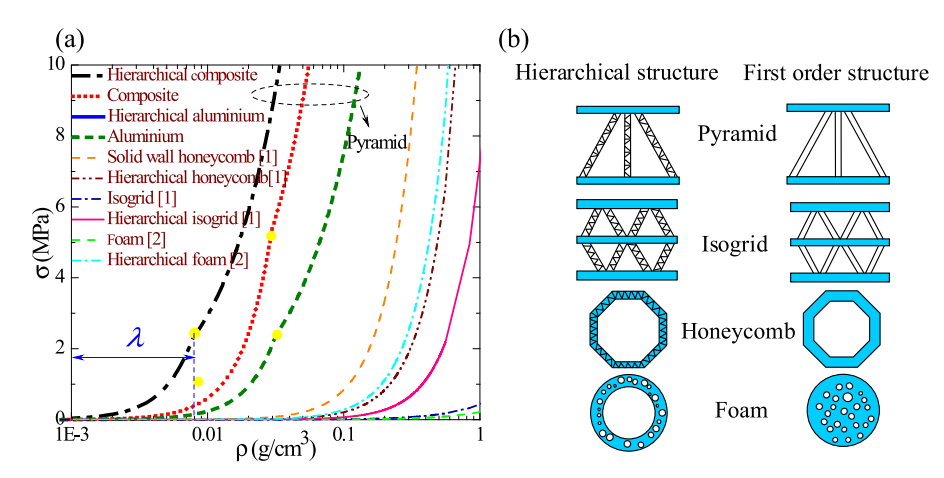


**Fig. 10.** The comparison of the out-of-plane compressive strength between the hierarchical and the first order sandwich structures in the literature. The line-dot shows the analytical data and the scattered points denote the experimental results. (a) Lattice and grid materials; (b) The schematic diagram of various structural configurations. Due to the small space in this diagram, the symbols [1]-[2] represent the papers which are listed in sequence in Section 3.5.3,  $\lambda$  denotes ultralight factor.

lent compressive performance of *pyramidal-pyramidal* hierarchical sandwich structures is more remarkable than that of the other structures with different topological configurations. For the listed structural configurations, only the pyramidal and hierarchical pyramidal structures in current study listed in Fig. 10(a) exist the ultralight factor. For the composite and aluminum pyramidal lattice truss in Fig. 10(a), the ultralight factors are 0.0299 and 0.0311. For the composite and aluminum pyramidal-pyramidal lattice truss, the ultralight factors are 0.0078 and 0.0084. Compared to other sandwich structures with various topological configurations, the magnitude of the ultralight factor  $\lambda$  of the pyramidal-pyramidal hierarchical sandwich structures is minimum. Therefore, based on the proposed concept of ideal ultralight weight sandwich materials, the hierarchical sandwich structure in this paper has excellent mechanical response under out-of-plane compression.

# 3.6. The equivalent shear stiffness

In order to obtain the relationship of external forces in truss members under shear loads, the in-plane shear force F is applied to the pyramidal unit cell as shown in Fig. 4(c). The expression between the resultant force F and the small displacement  $\delta$  associated with the shear force is (see Section 3.2.2 of the Appendix 3 for details)

$$F = \frac{4(EA)_e l^2 \cos^2 \alpha + 48(EI)_e \sin^2 \alpha}{l^3} \delta$$
 (23)

The axial force  $F_A$  along the truss member can be written as a function of the small displacement  $\delta$  as:

$$F_{A} = \frac{(EA)_{e}}{I} \delta \cos \alpha \tag{24}$$

where  $(EA)_e$  and  $(EI)_e$  are the equivalent compressive stiffness and equivalent flexural rigidity of the 1<sup>st</sup> order pyramidal lattice truss, respectively.

The relationship between the external shear force F of a unit cell and the axial force in truss member can be simplified as:

$$F = 4\xi_{\alpha}F_{A} \tag{25}$$

where the expression of dimensionless parameter  $\xi_{\alpha}$  in Eq. (25) is

$$\xi_{\alpha} = \frac{(EA)_e l^2 \cos^2 \alpha + 12(EI)_e \sin^2 \alpha}{(EA)_e l^2 \cos \alpha}$$
(26)

The equivalent shear stress  $\overline{\tau}$  and equivalent shear strain  $\overline{\nu}$  of a unit cell are

$$\bar{\tau} = \frac{2\xi_{\alpha}(EA)_e \cos \alpha}{l^3 \cos^2 \omega} \delta \tag{27}$$

$$\bar{\gamma} = \frac{\delta}{l \sin \omega} \tag{28}$$

The equivalent shear stiffness of the unit cell is  $\overline{G} = \overline{\tau}/\overline{\gamma}$ . Substituting Eqs. (27) and (28) into the equivalent shear stiffness expression, the shear stiffness can be further simplified as:

$$\overline{G} = \frac{2\xi_{\alpha}(EA)_{e}\cos\alpha\sin\omega}{l^{2}\cos^{2}\omega}$$
 (29)

In this section, the pyramidal sandwich panels according to various structural configurations of truss members are divided into two categories similar to the previous section. The pyramidal sandwich panels also include *pyramidal-pyramidal* hierarchical sandwich structures and the pyramidal sandwich structure with uniform cross-section truss members. The equivalent compressive stiffness and equivalent flexural rigidity of the hierarchical structures with *pyramidal-pyramidal* lattice trusses were obtained in Eqs. (11) and (12). Substituting Eqs. (11) and (12) into Eqs. (26) and (29), the equivalent out-of-plane shear stiffness of the hierarchical structures will be obtained in the next section. The derivation of the equivalent shear stiffness of the uniform cross-section lattice trusses can be found in Section 4.1 of the Appendix 4 in detail.

# 3.7. The equivalent shear strength

Based on the force analysis in Section 3.2.3.2 of the Appendix 3, the relationship between the shear force  $F_S$  (the bending moment M) and the axial force  $F_A$  through the free-body-diagram in our previous work, can be expressed as:

$$\frac{F_{\rm S}}{F_{\rm A}} = \frac{12(EI)_e \sin \alpha}{l^2(EA)_e \cos \alpha} \tag{30}$$

$$\frac{M}{F_A} = \frac{6(EI)_e \sin \alpha}{I(EA)_e \cos \alpha} \tag{31}$$

The relationship between the axial force of an arbitrary pyramidal truss member  $F_A^{oc}$  and the external shear force of the unit cell F is

$$F_A^{oc} = \frac{F}{4\xi_{cr}} (\sin \varphi + \cos \varphi) \tag{32}$$

where  $\varphi$  is the angle between the out-of-plane shear force and x-axis.

The truss members in pyramidal lattice cores shown in Fig. 2 are considered to be axially symmetrical. As shown in Fig. 2, the OD strut would likely undergo buckling or crushing failure when the angle is  $\pi/2 \le \varphi < \pi$ . Similarly, the collapse of the strut named OA will occur when the angle is  $\pi \le \varphi < 3\pi/2$ . The strut OB will buckle or collapse when the angle is  $3\pi/2 \le \varphi < 2\pi$ . In addition, the axial forces of struts are equal due to the geometrical distribution of struts. The pyramidal unit cell shows a specific failure mode when the external shear force is equal to *F*. The equivalent out-of-plane shear strength of the unit cell when the external force is equal to *F* can be expressed as:

$$\bar{\tau} = \frac{2F_A \xi_\alpha}{l^2 (\sin \varphi + \cos \varphi) \cos^2 \omega} \tag{33}$$

In Eqs. (A-13) and (A-14), both the face sheets and the pyramidal truss members are subjected to external in-plane compressive loads. In addition, the external force of the 2<sup>nd</sup> order pyramidal lattice core is related to the strut's geometric dimensions. Through a comprehensive analysis, four failure modes of the *pyramidal-pyramidal* hierarchical sandwich structures under shear force are identified. The corresponding equivalent shear strength of the hierarchical pyramidal unit cell under these failure modes is described as follows.

# 3.7.1. Face sheet wrinkling (FW) of the 2<sup>nd</sup> order lattice truss

The face sheet wrinkling has been described in Section 3.3, and the schematic diagram of this failure mode is shown in Fig. 5(a-III). The specific force analysis is described (see Section 4.2.1 of the Appendix 4 for details). Substituting Eq. (A-41) into Eq. (33), the equivalent shear strength of the hierarchical unit cell is

$$\bar{\tau} = \frac{\xi_{\alpha} (1 + \zeta_{p}) \pi^{2} E b t_{f}^{3}}{3 l_{c}^{2} l^{2} (\sin \varphi + \cos \varphi) \cos^{2} \beta \cos^{2} \omega}$$
(34)

# 3.7.2. Face sheet crushing (FC) of the 2<sup>nd</sup> order lattice truss

Similarly, the formula is derived in Section 4.2.2 of the Appendix 4. Substituting Eq. (A-42) into Eq. (33), the equivalent shear strength of the hierarchical unit cell is

$$\bar{\tau} = \frac{4\xi_{\alpha}(1+\zeta_{p})bt_{f}\sigma_{f}}{l^{2}(\sin\varphi + \cos\varphi)\cos^{2}\omega}$$
(35)

# 3.7.3. Core member buckling (CE) of the 2<sup>nd</sup> order lattice truss

The expression of the critical force of the  $2^{\rm nd}$  order truss member for the core member buckling of the  $2^{\rm nd}$  order lattice truss is described in Table 2. Substituting (EI)<sub>e</sub> =  $E\pi r_c^4/4$ , the axial force of the  $2^{\rm nd}$  order CE (Table 2) into Eq. (33), the corresponding equivalent shear strength of the unit cell is

$$\bar{\tau} = \frac{2\xi_{\alpha}\lambda_{p}\pi^{2}E\pi r_{c}^{4}}{l^{2}l_{c}^{2}(\sin\varphi + \cos\varphi)\cos^{2}\omega}$$
(36)

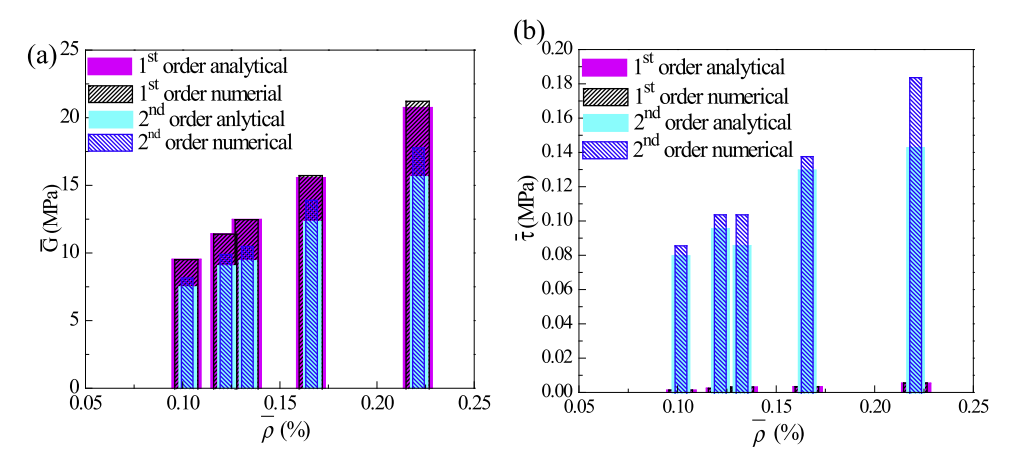


Fig. 11. Comparisons of shear properties between the 2<sup>nd</sup> order lattice truss and the 1<sup>st</sup> order pyramidal truss with different relative densities (the number of unit cells is equal to 51): (a) Shear stiffness; (b) Shear strength.

# 3.7.4. Macro Euler buckling of the 1<sup>st</sup> order lattice truss

The formula for the critical force of the Euler buckling of the strut is shown in Table 2. Substituting the axial force of the 1st order CE (Table 2) into Eq. (33), the equivalent shear strength of the unit cell is

$$\bar{\tau} = 8\xi_{\alpha} \frac{\pi^2 (EI)_e}{l^4 (\sin \varphi + \cos \varphi) \cos^2 \omega} \tag{37}$$

Similarly, the equivalent shear strength of the uniform cross-section lattice trusses under different failure modes has been derived in Section 4.2.2 of the Appendix 4.

# 3.8. Numerical simulation under shear loads

FE based computational models are used to investigate the shear properties of *pyramidal–pyramidal* hierarchical sandwich panels with details of computational parameters kept same with those under compressive load in Section 3.4. In addition, at least two elements were used along the width of the secondary pyramidal core struts. Fig. 11(a) shows the correspondence between the equivalent shear stiffness of the 1st and 2nd order lattice truss structures and relative density (0.102%–0.221%). Results show that the equivalent shear stiffness of the *pyramidal–pyramidal* 2nd order lattice truss structures is slightly lower than its 1st order counterpart. In contrast to the 1st order pyramidal truss structures in which all the members contribute almost equally to the overall shear stiffness of the structures, in the 2nd order lattice truss structures with the *pyramidal–pyramidal* lattice cores, greater part of the load is carried by the 2nd order face sheets and the contribution of corrugated struts is negligible. Thus, the equivalent shear stiffness of the 2nd order lattice truss structures is slightly lower than its 1st order counterpart of equal mass.

Fig. 11(b) shows the equivalent shear strength versus relative density (0.102%–0.221%) for both 1<sup>st</sup> and 2<sup>nd</sup> order lattice truss structures. Moreover, the corresponding magnitude of the equivalent shear strength is summarized in Table 7. As the relative density increases, the error between the theoretical and the numerical results of the hierarchical structure lies between 7.5% and 28.7%. The results show that the 2<sup>nd</sup> order structures are considerably stronger compared to the 1<sup>st</sup> order pyramidal truss structures in terms of shear strength. This is mainly due to a higher "anti-buckling" property (i.e., superior ability to resist buckling) of the 2<sup>nd</sup> order structures, where their bending stiffness is significantly greater than the 1<sup>st</sup> order pyramidal core of equal mass. This suggests that the 2<sup>nd</sup> order pyramidal core can better exploit the load-bearing capacity of the material compared to its 1<sup>st</sup> order counterpart.

#### 3.9. Comparative shear properties

In this section the equivalent shear stiffness of sandwich structures with various cross-sectional lattice trusses is compared. The equivalent shear strength of the hierarchical structures with uniform section lattice truss and self-similar pyramidal hierarchical structures in this paper are compared together. The shear strength of sandwich panels from the literature are included and compared to the results from the case studied in this paper.

# 3.9.1. Stiffness of pyramidal-pyramidal hierarchical lattice structures

In order to compare the shear stiffness of the hierarchical panels with uniform cross-section lattice truss, under the premise of ensuring the same weight, the equivalent shear stiffness of *pyramidal-pyramidal* hierarchical structure should

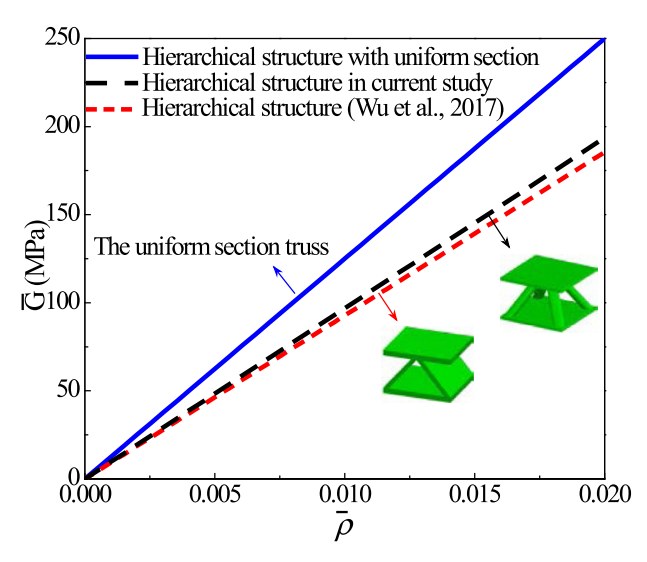


Fig. 12. Comparison of shear stiffness of hierarchical structures with corrugated, pyramidal truss sandwich struts and uniform sectional foam-core struts.

be expressed as a function of relative density. In addition, geometric parameters of the hierarchical struts should satisfy:  $t_f = ml_c$  and  $r_c = m^2l_c$ . Therefore, the equivalent shear stiffness of the structural hierarchy can be expressed as:

$$\overline{G} = \frac{1}{4} \xi_{\alpha} E f_p(m) \bar{\rho} \tag{38}$$

$$f_p(m) = \frac{8 + \pi m^3 + 9\pi m^7}{8(1 + 2\sqrt{2}m)(1 + 2\pi m^3)}$$
(39)

For lattice trusses with various sectional configurations, the relationship between the shear stiffness of sandwich structures and relative density is established in the derivation in Section 4.3.1 of the Appendix 4. The flexural rigidity of sandwich structures is closely related to the geometry of its structural section. For the pyramidal-pyramidal hierarchical structure, the 2<sup>nd</sup> order pyramidal strut is obtained by increasing the distance between the 2<sup>nd</sup> order face sheets to increase the core bending stiffness. In addition, the thickness of the 2<sup>nd</sup> order face sheets is much lesser than the distance of two face sheets, implying that the magnitude of m is very small. The equivalent shear stiffness versus relative density curve with m = 0.05is shown in Fig. 12. The shear stiffness of corrugated-pyramidal hierarchical sandwich panels in (Wu et al., 2017) were also included in Fig. 12. The stiffness of hierarchical structures with corrugated and pyramidal truss sandwich struts decreases about 14.6% and 12.5% compared with hierarchical structures with circular, triangular and rectangular struts, respectively as shown in Fig. 12. The increase in the stiffness is because all the materials of hierarchical structures with circular, triangular and square struts are used to bear the transformation. However, only face sheet of the 2<sup>nd</sup> order corrugated and pyramidal truss sandwich struts can be used to support load, and the core materials are used to increase the bending stiffness which only benefits the buckling resistance. The two hierarchical sandwich structures are only similar in terms of the structural equivalent stiffness. In fact, the 2<sup>nd</sup> order corrugated and pyramidal lattice trusses mainly increase the flexural rigidity of the 1st order struts using discrete materials, while the 2nd order core rod itself contributes little to the overall stiffness of the hierarchical structure. We now compare the equivalent shear stiffness of the self-similar pyramidal and corrugated-pyramidal hierarchical structures (Fig. 12). The equivalent shear stiffness of the two hierarchical sandwich structures in Eq. (38) are related to their corresponding geometrical characteristics. For the pyramidal-pyramidal hierarchical structure, since the pyramidal configuration is a stretching-dominated lattice material, the equivalent flexural rigidity of the structure in Eq. (26) is much smaller than the structural equivalent compressive stiffness, and the parameter in Eq. (38) satisfies  $\xi_{\alpha} \approx \cos \alpha$ . In Eq. (38), the parameter  $f_p(m)$  is related to the internal geometric parameters of the hierarchical structures. However, the elastic modulus of the parent material E equals 100 GPa and the magnitude of this parameter is much larger than that of  $f_p(m)$ . In other words, the parameter associated with the structural geometric dimensions contributes much less to the overall equivalent shear stiffness of the hierarchical structure than the elastic modulus of the parent materials. Similarly, the shear stiffness of the corrugated-pyramidal hierarchical structure is less affected by its geometric parameters as well.

#### 3.9.2. Strength of pyramidal-pyramidal hierarchical lattice structures

To compare the hierarchical panels with uniform cross-sectional truss members, the equivalent shear strength of pyramidal-pyramidal hierarchical structures should be expressed as a function of relative density under the premise of ensuring the same weight. Similarly, the geometric parameters also satisfy:  $t_f = ml_c$  and  $r_c = m^2 l_c$ . The corresponding failure

equation of face sheet crushing of the 2<sup>nd</sup> order lattice truss is

$$\bar{\tau}_{zy} + \bar{\tau}_{zx} = \xi_{\omega} (1 + \zeta_p) \sigma_f f_{fp}(m) \bar{\rho} \tag{40}$$

where the expression of parameter  $f_{fp}(m)$  in Eq. (40) has been described in Section 3.5.2.

The failure equation of macro Euler buckling of the 1st order pyramidal truss is

$$\bar{\tau}_{zy} + \bar{\tau}_{zx} = E\xi_{\omega}\pi^2 f_{bp}(m)\bar{\rho}^2 \tag{41}$$

where the expression of parameter  $f_{bp}(m)$  in Eq. (41) is Eq. (22).

The relationship between the equivalent shear strength of the uniform cross-section lattice trusses and relative density under different failure modes has been explained in detail in Section 4.3.2 of the Appendix 4. And this section describes the trends of the curves in Fig. 13(a)–(d). Fig. 13(e) shows the failure envelop curve of the equivalent shear strength with m = 0.1. The buckling collapses of hierarchical structures with circular, triangular and rectangular struts are also included in Fig. 13(e). The buckling resistant abilities of hierarchical structures with corrugated and pyramidal truss sandwich struts are considerably superior to that of hierarchical structures with circular, triangular and rectangular struts. The main reason is that the core material is only used to increase the bending stiffness of the sandwich panel, and pyramidal truss core is the lightest compared with other core materials or struts.

# 4. In-plane compression of pyramidal-pyramidal hierarchical sandwich structures

In this section, the in-plane compressive behavior of the *pyramidal-pyramidal* hierarchical sandwich panels will be investigated. Several failure modes are considered due to the structural hierarchy and the in-plane compressive loads. The dominant structural failure mode will change with the geometrical dimensions of the different parts of the structure. As shown in Fig. 5(b), five failure modes may occur during the in-plane compressive loading which is described as follows.

#### 4.1. Failure modes under in-plane compression

# 4.1.1. Macro Euler buckling of the pyramidal lattice truss

The hierarchical structure is composed of several numbers of *pyramidal–pyramidal* hierarchical lattice trusses, and the number of 1<sup>st</sup> order pyramidal truss is set to *n*. According to the basic mechanics of materials formulas, the critical loads in Euler buckling failure mode (Fig. 5(b-I)) is

$$F = \frac{\pi^2 (EI)_e}{2n^2 u^2 |^2 \cos^2 \omega} \tag{42}$$

where the parameter  $\mu = 0.5$  (Hearn, 1997). Substituting these expressions into Eq. (42), the critical loads of the hierarchical structures in this failure mode can be obtained accordingly.

# 4.1.2. Face sheet wrinkling (FW) of the 1st order pyramidal truss

For the case of face sheet wrinkling of the 1<sup>st</sup> order pyramidal truss (Fig. 5(b-II)), the critical load of the 1<sup>st</sup> order face sheet is in Table 2. Here, the flexural rigidity of the face sheet (EI)<sub>e</sub> equals to  $Ebt^3/12$ . The pyramidal lattice truss will deform during the in-plane compression, since the lattice struts are subject to the partial external force. Based on the effect of external forces, the total in-plane compressive load in this failure mode is

$$F = \frac{(1 + \xi_p)\pi^2(EI)_e}{\mu^2 I^2 \cos^2 \omega} \tag{43}$$

The expression for the non-dimensional parameter is defined as:

$$\xi_p = \frac{(EA)_e \cos^3 \beta}{(EA)_f} + \frac{12(EI)_e \sin^2 \beta \cos \beta}{(EA)_f l^2}$$
(44)

# 4.1.3. Face sheet crushing (FC) of the 1<sup>st</sup> order pyramidal truss

The flexural rigidity of the face sheets increases with increasing their designed thickness, improving their anti-buckling feature. The failure modes of composite materials will be divided into two categories: the Euler buckling and the crushing of the composite materials. The average strength of the face sheet's crushing is defined as  $\sigma_f$ , and this stress value can be measured by compressive tests. Because the two face sheets are the same, the critical external load in collapse of the 1<sup>st</sup> order face sheets (Fig. 5(b-III)) is

$$F = 4\sqrt{2}\sigma_f lt_f \cos \omega \tag{45}$$

The relationship between the external force on the face sheets  $F_f$  and the general in-plane compressive loads F can be expressed as:

$$F = 4\sqrt{2}(1+\xi_p)\sigma_f lt_f \cos \omega \tag{46}$$

where the expression of parameter  $\xi_p$  is described in Eq. (A-13).

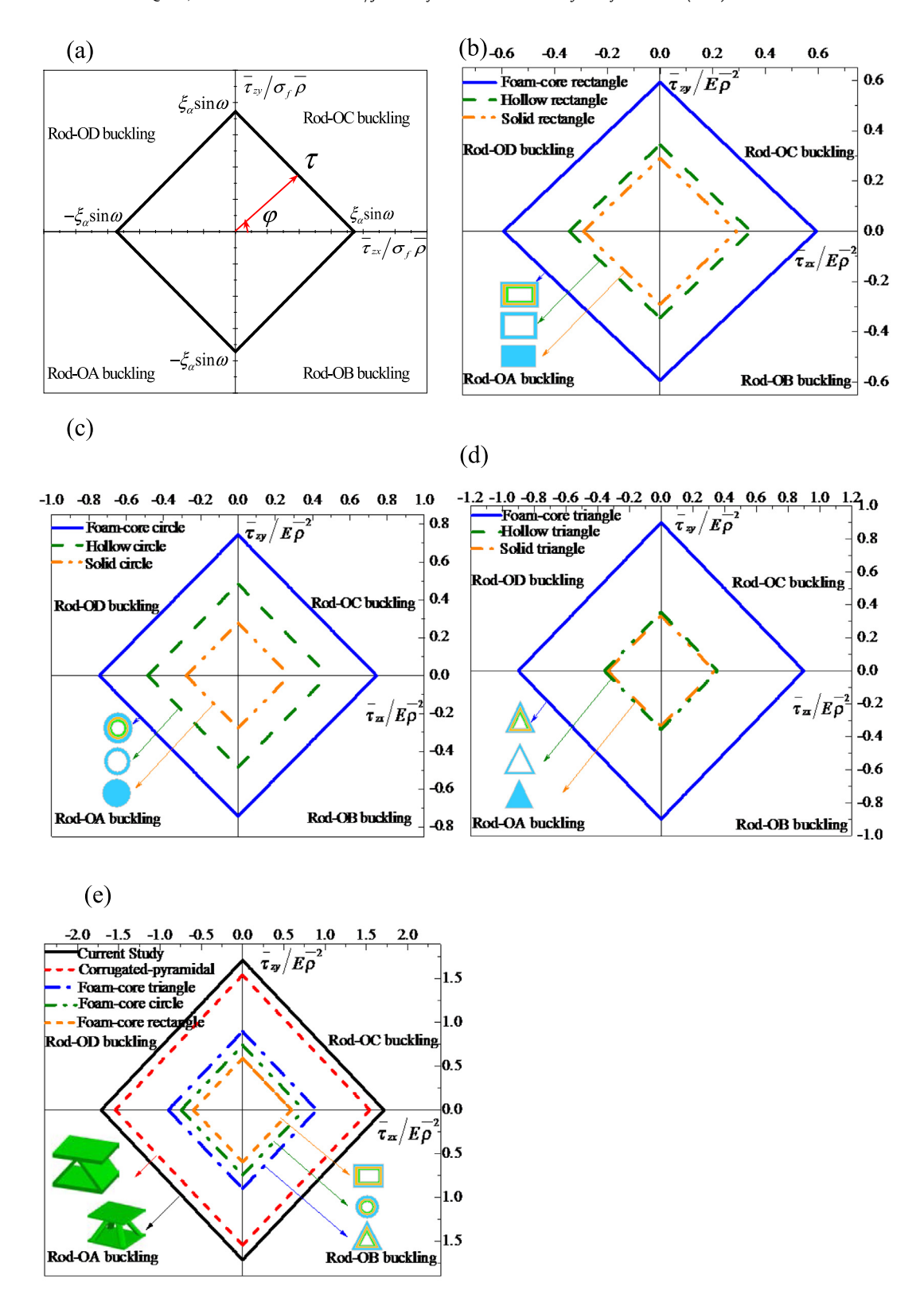


**Fig. 13.** The aggregate shear properties of hierarchical sandwich structures: (a) crushing failure collapse of hierarchical structures with circular, rectangular and triangular struts, (b) shear buckling failure collapse map of hierarchical structures with rectangular cross-section, (c) shear buckling failure collapse map of hierarchical structures with circular cross-section, (d) shear buckling failure collapse map of hierarchical structures with triangular cross-section, (e) the shear properties of hierarchical sandwich structures: comparisons of shear buckling strength of hierarchical structures with different struts.

# 4.1.4. Face sheet wrinkling (FW) of the 2<sup>nd</sup> order lattice truss

For wrinkling of the  $2^{\text{nd}}$  order face sheets (Fig. 5(b-IV)), the total external force  $P_c$  of the face sheets under this failure mode is in Table 2. Here, the flexural rigidity of the face sheet  $(EI)_e$  equals to  $Ebt_f^3/12$ . The axial force along the  $1^{\text{st}}$  order pyramidal struts can be formulated as:

$$F_A = (1 + \xi_{CD})P_C \tag{47}$$

where the non-dimensional parameter is

$$\xi_{cp} = \frac{(EA)_{cp} \cos^3 \beta}{(EA)_{cf}} + \frac{12(EI)_{cp} \sin^2 \beta \cos \beta}{(EA)_{cf} l^2}$$
(48)

In Eq. (48),  $(EA)_{cf}$  denotes the equivalent compressive stiffness of the 1<sup>st</sup> order face sheets  $(EA)_{cf} = Eb_ct_f$ .  $(EA)_{cp}$  is the equivalent compressive stiffness of the 2<sup>nd</sup> order pyramidal truss members  $(EA)_{cp} = E\pi r_c^2$ .  $(EI)_{cp}$  is the equivalent flexural rigidity of the 2<sup>nd</sup> order pyramidal struts  $(EI)_{cp} = E\pi r_c^4/4$ .

Through the relationship between the axial force of a single pyramidal strut and total in-plane compressive load, the total in-plane compressive load of the hierarchical structure is

$$F = \frac{\lambda_p (1 + \xi_{cp}) \pi^2 E b t_f^3}{3 l_c^2 \cos^2 \omega} \tag{49}$$

where the parameter  $\lambda_p$  in Eq. (49) is

$$\lambda_p = 2\cos\beta + \frac{2(EA)_f}{(EA)_p \cos^2\beta} + \frac{24(EI)_p \sin^2\beta}{(EA)_p I^2 \cos\beta}$$
 (50)

The terms  $(EA)_p$  and  $(EI)_p$  are the equivalent compressive stiffness and the equivalent flexural rigidity of the pyramidal lattice truss, respectively.  $(EA)_f$  denotes the equivalent compressive stiffness of the face sheets.

# 4.1.5. Face sheet crushing (FC) of the 2<sup>nd</sup> order lattice truss

The crushing strength of composite materials is that of the raw material used in the preparation of structures and denoted by  $\sigma_f$ . The corresponding axial force  $F_{cf}$  in the 2<sup>nd</sup> order face sheet for the face sheet crushing of the 2<sup>nd</sup> order lattice truss (Fig. 5(b-V)) is in Table 2. According to the relationship between the load in face sheets and the axial force along truss members, the axial force along the 1<sup>st</sup> order pyramidal lattice truss is

$$F_A = (1 + \xi_{cp})F_{cf} \tag{51}$$

The total in-plane load of the hierarchical structure can be deduced in accordance with the relationship between the axial force along the lattice truss and in-plane compressive load as:

$$F = 2\lambda_p (1 + \xi_{cp}) b t_f \sigma_f \tag{52}$$

# 4.2. The failure mechanism map under in-plane compression

In order to demonstrate the relationship between the geometrical dimensions and the failure modes of the hierarchical sandwich panels, the failure mechanism maps of sandwich structures under in-plane compression are plotted based on the failure modes described in Section 4.1. The inclination angles between the 1<sup>st</sup> order or 2<sup>nd</sup> order pyramidal struts with their corresponding face sheets are considered to be 45° for both  $\omega$  and  $\omega_c$ . For the design of the hierarchical structures, several geometric parameters are significant including the thickness of the hierarchical sandwich panels T, the thickness of the 2<sup>nd</sup> order face sheets  $t_f$ , the radius and length of the 2<sup>nd</sup> order pyramidal truss member  $r_c$  and  $l_c$  respectively. The number of pyramidal–pyramidal hierarchical unit cell is  $n_l^2$  along the length of the 1<sup>st</sup> order lattice truss, and the number of the 2<sup>nd</sup> order pyramidal unit cell is  $n_l^1$  along the length of hierarchical sandwich structures. The parameter  $n_w^2$  denotes the number of the 2<sup>nd</sup> order lattice truss along the width of the 1<sup>st</sup> order pyramidal lattice truss. The dimensionless parameters  $r_c/l_c$ ,  $T/l_c$  and  $t_f/l_c$  are regarded as x-axis, y-axis and z-axis, respectively to plot the failure mechanism maps. The parameters  $n_l^1$  and  $n_l^2$  are defined as variable parameters affecting the change of the boundary of each failure mode.

Fig. 14 shows three cases: (1)  $n_w^2 = 1$ ,  $n_l^2 = 5$ ,  $n_l^1 = 10$ ; (2)  $n_w^2 = 1$ ,  $n_l^2 = 5$ ,  $n_l^1 = 50$  and (3)  $n_w^2 = 1$ ,  $n_l^2 = 8$ ,  $n_l^1 = 10$ . As shown in Fig. 15, the variation of curve's positions on the failure mechanism maps has a close relationship with the parameters  $n_l^1$  and  $n_l^2$ . The aforesaid non-dimensional parameters which are regarded as three sets of coordinate axes codetermine the location of each failure mode. In addition, the larger the area occupied by the failure mode, the more likely the failure mode will occur. From Fig. 14(a)–(c), the face sheet wrinkling of the  $2^{nd}$  order lattice truss can be regarded as the dominant failure mode owing its largest volume in the failure mechanism maps. The local buckling of the  $2^{nd}$  order face sheets appear on account of the greater distance between adjacent nodes in the  $2^{nd}$  order lattice truss and in that case the corresponding face sheet wrinkling of the  $2^{nd}$  order lattice truss is likely to occur. From Fig. 14(a) and (b), the possibility of the face sheet crushing of the  $2^{nd}$  order lattice truss is reduced with the increase in the number of the  $1^{st}$  order pyramidal unit cell along

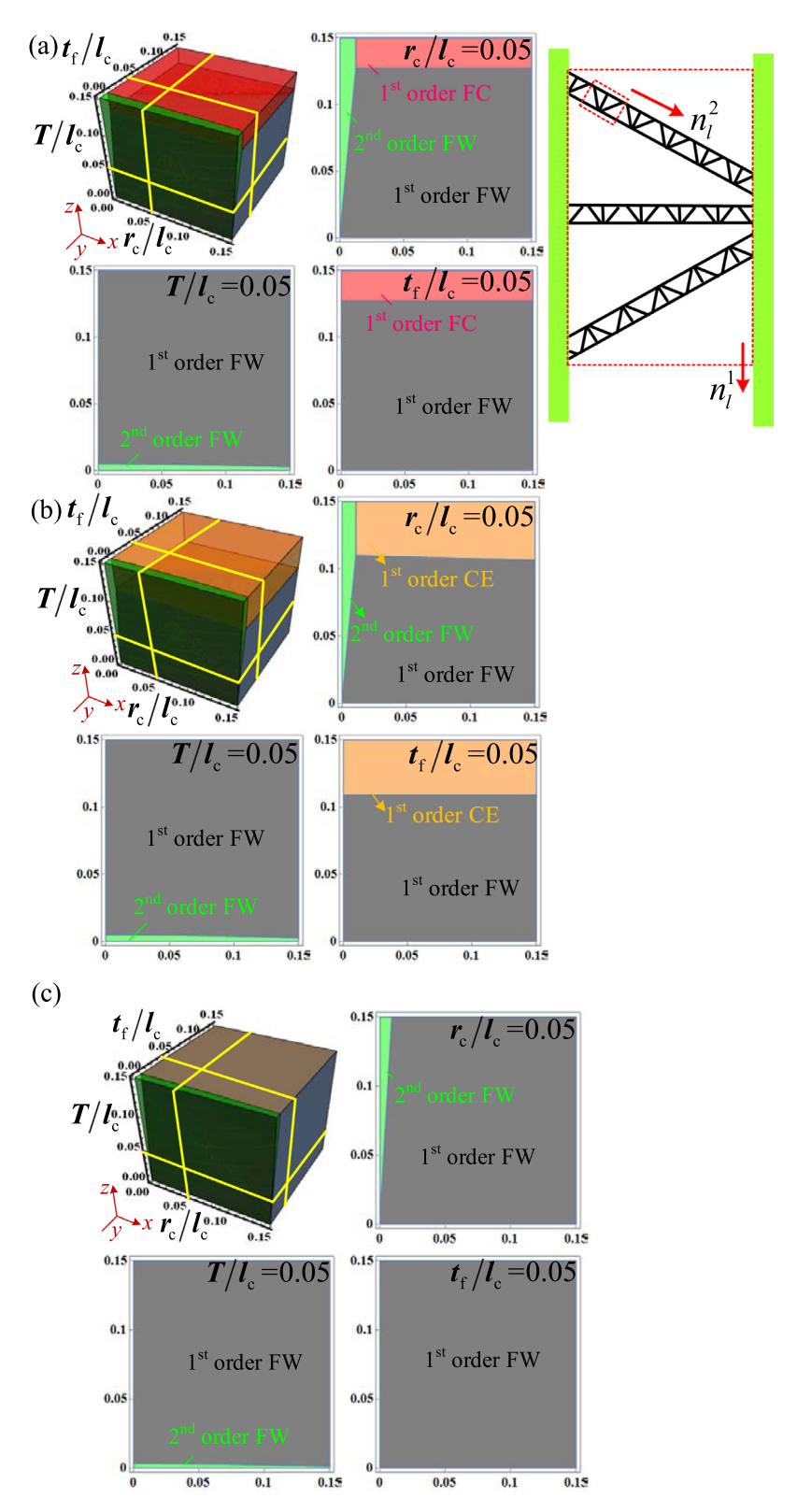


**Fig. 14.** The failure mechanism maps of the *pyramidal–pyramidal* hierarchical sandwich structures under in-plane compressive loads in three cases (i.e. The failure mode can be changed by changing the number of the 1<sup>st</sup> order and 2<sup>nd</sup> order unit cells): The number of 2<sup>nd</sup> order unit cell along the length of 1<sup>st</sup> order lattice truss  $(n_l^2)$  and that of the 1<sup>st</sup> order unit cell along the length of 1<sup>st</sup> order face sheet  $(n_l^1)$  are (a) 5 and 10; (b) 5 and 50; and (c) 8 and 10 respectively.

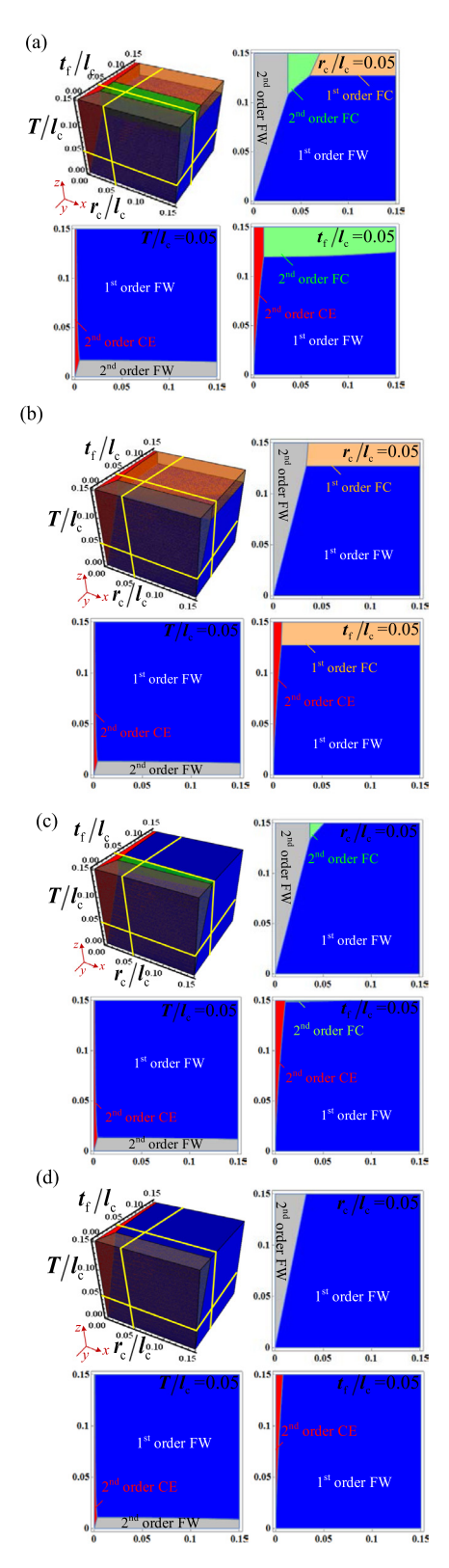


**Fig. 15.** The failure mechanism maps of the *pyramidal-pyramidal* hierarchical sandwich structures under three-point bending loads in four cases (i.e. The failure mode can be changed by changing the number of 1<sup>st</sup> order and 2<sup>nd</sup> order unit cells): The number of 2<sup>nd</sup> order unit cell along the length of 1st order lattice truss  $(n_l^2)$  and that of the 1<sup>st</sup> order unit cell along the length of 1<sup>st</sup> order face sheet  $(n_l^1)$  are (a) 5 and 5; (b) 5 and 10; (c) 10 and 5; (d) 10 and 10 respectively.

**Table 1** Equivalent out-of-plane compressive strength of the pyramidal unit cell with different cross-sections.

Sectional properties	Equivalent buckling strength $(\overline{\sigma}/\text{MPa})$	Equivalent crushing strength $(\overline{\sigma}/\mathrm{MPa})$
Solid rectangle	$\frac{2\xi_{\omega}\pi^{2}Ebh^{3}}{3l^{4}\cos^{2}\omega}$	$\frac{2\xi_{\omega}\sigma_{f}bh}{l^{2}\cos^{2}\omega}$
Hollow rectangle	$\frac{2E\xi_{\omega}\pi^{2}(bh^{3}-b_{1}h_{1}^{3})}{3l^{4}\cos^{2}\omega}$	$\frac{2\xi_{\omega}\sigma_{f}(bh-b_{1}h_{1})}{l^{2}\cos^{2}\omega}$
Foam rectangle	$\frac{2E\xi_{\omega}\pi^{2}(b_{4}h_{4}^{2}-b_{3}h_{3}^{2}+b_{2}h_{2}^{2}-b_{1}h_{1}^{3})}{3l^{4}\cos^{2}\omega}$	$\frac{2\xi_{\omega}\sigma_f(b_4h_4-b_3h_3+b_2h_2-b_1h_1)}{l^2\cos^2\omega}$
Solid circle	$\frac{2\pi^3 \xi_{\omega} ER^4}{l^4 \cos^2 \omega}$	$\frac{2\xi_{\omega}\sigma_f\pi R^2}{I^2\cos^2\omega}$
Hollow circle	$\frac{2\pi^3\xi_\omega E(R^4-r^4)}{l^4\cos^2\omega}$	$\frac{2\xi_{\omega}\sigma_{f}\pi(R^{2}-r^{2})}{l^{2}\cos^{2}\omega}$
Foam circle	$\frac{2\pi^{3}\xi_{\omega}E(r_{4}^{4}-r_{3}^{4}+r_{1}^{4}-r_{1}^{4})}{l^{4}\cos^{2}\!\omega}$	$\frac{2\xi_{\omega}\sigma_{f}\pi(r_{4}^{2}-r_{3}^{2}+r_{2}^{2}-r_{1}^{2})}{I^{2}\cos^{2}\omega}$
Solid triangle	$\frac{\sqrt{3}\xi_{\omega}\pi^2Ed^4}{12l^4\cos^2\omega}$	$\frac{\sqrt{3}\xi_{\omega}\sigma_{f}a^{2}}{2l^{2}\cos^{2}\omega}$
Hollow triangle	$\frac{\sqrt{3}E\xi_{\omega}\pi^{2}(a^{4}-a_{1}^{4})}{12l^{4}\cos^{2}\omega}$	$\frac{\sqrt{3}\xi_{\omega}\sigma_f(a^2-a_1^2)}{2l^2\cos^2\omega}$
Foam triangle	$\frac{\sqrt{3} E \xi_{\omega} \pi^2 (a_4^4 \!-\! a_3^4 \!+\! a_2^4 \!-\! a_1^4)}{12 l^4 cos^2 \omega}$	$\frac{\sqrt{3}\xi_{\omega}\sigma_{f}(a_{4}^{2}-a_{3}^{2}+a_{2}^{2}-a_{1}^{2})}{2l^{2}\cos^{2}\omega}$

**Table 2** Equivalent compressive strength of the hierarchical pyramidal sandwich structure under each failure mode.

	2 <sup>nd</sup> order FW	2 <sup>nd</sup> order FC	2 <sup>nd</sup> order CE	1 <sup>st</sup> order CE
Critical load-F	$\frac{\pi^2(EI)_e}{\mu^2 l_c^2 \cos^2 \omega}$	$2bt_f\sigma_f$	$\frac{\pi^2(EI)_e}{\mu^2 l_c^2}$	-
Axial force- $F_A$	$\frac{(1+\xi_p)\pi^2 Ebt_f^3}{3l_c^2\cos^2\omega}$	$2(1+\xi_p)bt_f\sigma_f$	$\frac{\pi^2(EI)_e \lambda_p}{\mu^2 l_c^2}$	$\frac{\pi^2(EI)_e}{\mu^2l^2}$
$ECS^a$ - $\sigma$	$\frac{2\xi_{\omega}(1+\xi_p)\pi^2Ebt_f^3}{3l^2l_c^2\cos^4\omega}$	$\frac{4\xi_{\omega}(1+\xi_{p})bt_{f}\sigma_{f}}{l^{2}\cos^{2}\omega}$	$\frac{2\xi_{\omega}\lambda_{p}\pi^{2}E\pi r_{c}^{4}}{l^{2}l_{c}^{2}\cos^{2}\omega}$	$\frac{8\xi_{\omega}\pi^{2}(EI)_{e}}{I^{4}\cos^{2}\omega}$

<sup>&</sup>lt;sup>a</sup> The abbreviation ECS denotes the equivalent compressive strength.

**Table 3** Equivalent compressive strength of the pyramidal unit cell with different types of cross-sections.

Sectional properties	Solid	Hollow	Foam core
Equivalent compressive strength $(\overline{\sigma}/\text{MPa})$	$\frac{\xi_{\omega}E\pi}{8}\bar{ ho}^2$	$\frac{\xi_{\omega} E \pi f_h(g_h)}{8} \bar{\rho}^2$	$\frac{\xi_{\omega} E \pi f_m(g_f)}{8} \bar{\rho}^2$

**Table 4** Equivalent shear stiffness of the pyramidal unit cell with different types of cross-sections.

Sectional properties	Dimensionless parameter $(\xi_{\alpha})$	Equivalent shear stiffness (G/MPa)
Solid rectangle	$\cos \alpha + \frac{h^2 \sin^2 \alpha}{l^2 \cos \alpha}$	$\frac{2\xi_{\alpha}Ebh\sin^{2}\omega}{l^{2}\cos^{2}\omega}$
Hollow rectangle	$\cos \alpha + \frac{(bh^3 - b_1h_1^3)\sin^2\alpha}{(bh - b_1h_1)l^2\cos\alpha}$	$\frac{2\xi_{\alpha}E(bh-b_1h_1)\cos\alpha\sin\omega}{l^2\cos^2\omega}$
Foam rectangle	$\cos \alpha + \frac{(b_4 h_4^3 - b_3 h_3^3 + b_2 h_3^3 - b_1 h_3^3) \sin^2 \alpha}{(b_4 h_4 - b_3 h_3 + b_2 h_2 - b_1 h_1) l^2 \cos \alpha}$	$\frac{2\xi_{\alpha}E(b_4h_4-b_3h_3+b_2h_2-b_1h_1)\cos\alpha\sin\omega}{l^2\cos^2\omega}$
Solid circle	$\cos \alpha + \frac{3R^2 \sin^2 \alpha}{l^2 \cos \alpha}$	$\frac{2\pi \xi_{\alpha} ER^2 \cos \alpha \sin \omega}{l^2 \cos^2 \omega}$
Hollow circle	$\cos \alpha + \frac{3(R^2+r^2)\sin^2 \alpha}{l^2\cos \alpha}$	$\frac{2\pi\xi_{\alpha}E(R^2-r^2)\cos\alpha\sin\omega}{l^2\cos^2\omega}$
Foam circle	$\cos \alpha + \frac{3(r_4^4 - r_3^4 + r_2^4 - r_1^4)\sin^2 \alpha}{(r_4^2 - r_3^2 + r_2^2 - r_1^2)l^2\cos \alpha}$	$\frac{2\pi\xi_{\alpha}E(r_{4}^{2}-r_{3}^{2}+r_{2}^{2}-r_{1}^{2})\cos\alpha\sin\omega}{l^{2}\!\cos^{2}\!\omega}$
Solid triangle	$\cos \alpha + \frac{a^2 \sin^2 \alpha}{2l^2 \cos \alpha}$	$\frac{\sqrt{3}\xi_{\alpha}Ea^{2}\cos\alpha\sin\omega}{2l^{2}\cos^{2}\omega}$
Hollow triangle	$\cos\alpha + \frac{(a^2 + a_1^2)\sin^2\alpha}{2l^2\cos\alpha}$	$\frac{\sqrt{3}\xi_{\alpha}E(a^2-a_1^2)\cos\alpha\sin\omega}{2l^2\cos^2\omega}$
Foam triangle	$\cos \alpha + \frac{(a_4^4 - a_3^4 + a_2^4 - a_1^4)\sin^2 \alpha}{2(a_4^2 - a_3^2 + a_2^2 - a_1^2)l^2\cos \alpha}$	$\frac{\sqrt{3}\xi_{\alpha}E(a_4^2-a_3^2+a_2^2-a_1^2)\cos\alpha\sin\omega}{2l^2\cos^2\omega}$

the length of hierarchical sandwich panels. In contrast, the possibility of macro Euler buckling of pyramidal lattice truss is greatly increased with the increase in the number of the 1<sup>st</sup> order pyramidal unit cell. Similarly, Fig. 14(a) and (c) show that the position of face sheet crushing of the 2<sup>nd</sup> order lattice truss will be replaced by face sheet wrinkling of the 1<sup>st</sup> order lattice truss as the parameter,  $n_l^2$ , increases. The reason is that under the same in-plane compressive load, the local buckling of the 1<sup>st</sup> order pyramidal lattice struts, namely, the face sheet wrinkling of the 2<sup>nd</sup> order lattice truss, is more likely to occur as the length of the 1<sup>st</sup> order pyramidal truss increases.

# 5. Three-point bending of pyramidal-pyramidal hierarchical sandwich structures

In this section, the face sheets of sandwich structures are subjected to bending moment. The face sheet wrinkling and the face sheet crushing failure modes are the potential failure modes for this loading state. However, the *pyramidal-pyramidal* 

**Table 5** Equivalent shear strength of the pyramidal unit cell with uniform sectional shapes.

Sectional properties	Equivalent buckling strength $(\overline{\tau}/\text{MPa})$	Equivalent crushing strength $(\overline{\tau}/\text{MPa})$
Solid rectangle	$\frac{2\xi_{\alpha}\sigma_{f}bh}{l^{2}(\sin\varphi+\cos\varphi)\cos^{2}\omega}$	$\frac{2\xi_{\alpha}\pi^{2}Ebh^{3}}{3l^{4}(\sin\varphi+\cos\varphi)\cos^{2}\omega}$
Hollow rectangle	$\frac{2E\xi_{\alpha}\pi^{2}(bh^{3}-b_{1}h_{1}^{3})}{3l^{4}(\sin\varphi+\cos\varphi)\cos^{2}\omega}$	$\frac{2\xi_{\alpha}\sigma_{f}(bh-b_{1}h_{1})}{l^{2}(\sin\varphi+\cos\varphi)\cos^{2}\omega}$
Foam rectangle	$\frac{2E\xi_{\alpha}\pi^{2}(b_{4}h_{4}^{3}-b_{3}h_{3}^{3}+b_{2}h_{3}^{3}-b_{1}h_{3}^{3})}{3l^{4}(\sin\varphi+\cos\varphi)\cos^{2}\omega}$	$\frac{2\xi_{\alpha}\sigma_{f}(b_{4}h_{4}-b_{3}h_{3}+b_{2}h_{2}-b_{1}h_{1})}{l^{2}(\sin\varphi+\cos\varphi)\cos^{2}\omega}$
Solid circle	$\frac{2\xi_{\alpha}\sigma_{f}\pi R^{2}}{l^{2}(\sin\varphi+\cos\varphi)\cos^{2}\omega}$	$\frac{2\pi^3 \xi_{\alpha} ER^4}{I^4 (\sin \varphi + \cos \varphi) \cos^2 \omega}$
Hollow circle	$\frac{2\pi^3 \xi_{\alpha} E(R^4 - r^4)}{l^4 (\sin \varphi + \cos \varphi) \cos^2 \omega}$	$\frac{2\xi_{\omega}\sigma_{f}\pi\left(R^{2}-r^{2}\right)}{l^{2}(\sin\varphi+\cos\varphi)\cos^{2}\omega}$
Foam circle	$\frac{2\pi^{3}\xi_{\omega}E(r_{4}^{4}-r_{3}^{4}+r_{2}^{4}-r_{1}^{4})}{l^{4}(\sin\varphi+\cos\varphi)\cos^{2}\omega}$	$\frac{2\xi_{\alpha}\sigma_{f}\pi\left(r_{4}^{2}-r_{3}^{2}+r_{2}^{2}-r_{1}^{2}\right)}{l^{2}(\sin\varphi+\cos\varphi)\cos^{2}\omega}$
Solid triangle	$\frac{\sqrt{3}\xi_{\alpha}\sigma_{f}a^{2}}{2l^{2}(\sin\varphi+\cos\varphi)\cos^{2}\omega}$	$\frac{\sqrt{3}\xi_{\alpha}\pi^{2}Ea^{4}}{12l^{4}(\sin\varphi+\cos\varphi)\cos^{2}\omega}$
Hollow triangle	$\frac{\sqrt{3}E\xi_{\alpha}\pi^{2}(a^{4}-a_{1}^{4})}{12I^{4}(\sin\varphi+\cos\varphi)\cos^{2}\omega}$	$\frac{\sqrt{3}\xi_{\alpha}\sigma_{f}(a^{2}-a_{1}^{2})}{2l^{2}(\sin\varphi+\cos\varphi)\cos^{2}\omega}$
Foam triangle	$\frac{\sqrt{3}E\xi_{\alpha}\pi^{2}(a_{4}^{4}-a_{3}^{4}+a_{2}^{4}-a_{1}^{4})}{12l^{4}(\sin\varphi+\cos\varphi)\cos^{2}\omega}$	$\frac{\sqrt{3}\xi_{\alpha}\sigma_{f}(a_{4}^{2}-a_{3}^{2}+a_{2}^{2}-a_{1}^{2})}{2l^{2}(\sin\varphi+\cos\varphi)\cos^{2}\omega}$

**Table 6** Compressive strength of  $2^{nd}$  order lattice truss and  $1^{st}$  order pyramidal truss with different relative densities (MPa)  $(n_l^1 = 51, n_l^2 = 2)$ .

$\overline{ ho}(\%)$	1st order analytical	1st order numerical	2 <sup>nd</sup> order analytical	2 <sup>nd</sup> order numerical
0.102	0.0035	0.0036	0.253	0.21
0.122	0.0061	0.0061	0.306	0.252
0.133	0.0079	0.0079	0.29	0.254
0.166	0.0083	0.0084	0.418	0.332
0.221	0.0131	0.0133	0.483	0.439

**Table 7** Shear strength of  $2^{\rm nd}$  order lattice truss and  $1^{\rm st}$  order pyramidal truss with different relative densities (MPa)  $(n_l^1=51,n_l^2=2)$ .

$\overline{ ho}(\%)$	1st order analytical	1st order numerical	2 <sup>nd</sup> order analytical	2 <sup>nd</sup> order numerical
0.102	0.0014	0.0015	0.08	0.086
0.122	0.0025	0.0025	0.096	0.104
0.133	0.0032	0.0033	0.086	0.104
0.166	0.0034	0.0035	0.13	0.138
0.221	0.0054	0.0056	0.143	0.184

hierarchical lattice trusses also experience shear loads increasing the possibility of the four failure modes depicted in Section 3.7 to occur. Fig. 5(c) shows the four failure modes of the pyramidal lattice cores including face sheet wrinkling of the  $1^{st}$  order lattice truss, face sheet crushing of the  $1^{st}$  order lattice truss, face sheet crushing of the  $2^{nd}$  order lattice truss and face sheet crushing of the  $2^{nd}$  order lattice truss. In the next section, the corresponding structural strength terms for the failure modes in the three-point bending configuration are derived.

# 5.1. Failure modes under three-point bending conditions

# 5.1.1. Face sheet wrinkling (FW) of the 1st order pyramidal lattice truss

The expression for the failure mode of *pyramidal–pyramidal* hierarchical truss members under three-point bending loads can be derived and the external loads of hierarchical pyramidal sandwich panels can be expressed as:

$$F = \frac{4\pi^2 t^3 E \sin \omega}{3n l \cos^2 \omega} \tag{53}$$

where n denotes the number of the 1<sup>st</sup> order unit cell in hierarchical sandwich structures. The residual parameters in Eq. (53) have been described in aforesaid sections.

#### 5.1.2. Face sheet crushing (FC) of the 1<sup>st</sup> order pyramidal lattice truss

The external loads of pyramidal lattice structures under this failure mode is

$$F = -\frac{4}{n}\sin\omega\sigma_f lt \tag{54}$$

where the related parameters have been introduced in the previous sections.

# 5.1.3. Face sheet wrinkling (FW) of the $2^{nd}$ order lattice truss

The external load associated with this failure mode equals the out-of-plane compressive strength of the structures under FW of the 2<sup>nd</sup> order lattice truss in Section 3.3.2 multiplied by the area of the 1<sup>st</sup> order pyramidal unit cell. Therefore, the corresponding expression of external loads can be expressed as:

$$F = \frac{2\xi_{\omega}(1 + \xi_{c})\pi^{2}Ebt_{f}^{3}}{3l_{c}^{2}\cos^{2}\omega}$$
 (55)

# 5.1.4. Face sheet crushing (FC) of the 2<sup>nd</sup> order pyramidal truss

Similarly, the external loads of pyramidal-pyramidal hierarchical unit cell associated with collapse of the  $2^{nd}$  order face sheets is

$$F = 8\xi_{\omega}(1 + \xi_c)bt_f\sigma_f \tag{56}$$

# 5.2. The failure mechanism map under three-point bending conditions

This section describes four scenarios of hierarchical sandwich structures with various numbers of unit cells under three-point bending loads, namely, (1)  $n_w^2 = 1$ ,  $n_l^2 = 5$ ,  $n_l^1 = 5$ ; (2)  $n_w^2 = 1$ ,  $n_l^2 = 5$ ,  $n_l^1 = 10$ ; (3)  $n_w^2 = 1$ ,  $n_l^2 = 10$ ,  $n_l^1 = 5$ ; (4)  $n_w^2 = 1$ ,  $n_l^2 = 10$ ,  $n_l^1 = 10$ . The corresponding three-dimensional failure mechanism map is shown in Fig. 15 demonstrating the effect of the numbers of single-cell on the failure modes. As shown in Fig. 15, the number of the 1<sup>st</sup> or 2<sup>nd</sup> order unit cell affects the slenderness ratio of the 1<sup>st</sup> order lattice truss and the distribution of failure mode location.

The area enclosed by the threshold of each failure mode constitutes the failure mechanism map. The occurrence of a particular failure mode is directly related to the area occupied by the failure mode. The five failure modes where the face sheet wrinkling of the  $2^{nd}$  order lattice truss is the dominant failure mode is shown in Fig. 15(a) which compares the volume size of each failure mode in the failure mechanism map. In addition, grey area in this figure indicates the face sheet wrinkling of the  $1^{st}$  order lattice truss. Namely, the dimensionless parameter  $t_f/l_c$  satisfies less than 0.25, and the corresponding thickness of  $2^{nd}$  order face sheets is relatively small. Based on this observation, this failure mode will be observed during three-point bending. Similarly, core member buckling of the  $2^{nd}$  order lattice truss occurs in some cases where the parameter ratio  $r_c/l_c$  is less than 0.015.

As shown in Fig. 15(b), the face sheet crushing of the 1<sup>st</sup> order lattice truss vanishes with an increase in the number of 1<sup>st</sup> order pyramidal unit cells. Fig. 15(c) and (d) support the same observation. The face sheet wrinkling of 2<sup>nd</sup> order lattice truss is mainly caused by localized bulking of face sheets of the 2<sup>nd</sup> order pyramidal truss between adjacent nodes. Fig. 15(a) through 15(d) suggest that the face sheet wrinkling of 2<sup>nd</sup> order lattice truss can be regarded as a dominate failure mode under three-point bending loads. The reason is that the 2<sup>nd</sup> order lattice truss can be regarded as a slender rod when the parameter ratio  $r_c/l_c$  is less than 0.15. Furthermore, Fig. 15(a)–(d) show that core member buckling (CE) of the 2<sup>nd</sup> order lattice truss becomes a factor when the parameter value  $r_c/l_c$  is minimum. By comparing the volume size of possible failure mode in Fig. 15, this failure mode is very unlikely to appear.

# 6. Conclusions

In this paper, we propose the concept of an ideal ultralight weight sandwich materials and introduce the *pyramidal-pyramidal* topological configuration for hierarchical sandwich structures. The mechanical response and failure of the *pyramidal-pyramidal* 2<sup>nd</sup> order lattice truss structures under different quasi-static loading conditions were investigated through analytical and numerical methods. In addition, the effect of the cross-sectional characteristics of the lattice truss on the mechanical properties of sandwich structures was explored. The out-of-plane compressive strength of sandwich structures from other literatures was compared to that of the hierarchical *pyramidal-pyramidal* sandwich materials in this paper. The results indicated a good correlation between analytical predictions and FE simulations. Based on the proposed concept of ideal ultralight weight sandwich materials, the mechanical properties of hierarchical structures were shown to have significant advantages compared to the 1<sup>st</sup> order sandwich structures. Also by comparing the hierarchical structures from the literature to the proposed hierarchical sandwich structure, we highlighted the superior mechanical performance of the *pyramidal-pyramidal* sandwich materials.

#### Acknowledgments

The present work was supported in part by the National Science Foundation of China under grant Nos. 11572100, 11302060, 11432004 and 11421091, and in part by the United States National Science Foundation, CMMI Grant No. 1634560 (AV and MEA). JX was support by Program for Outstanding Young Scholars in Harbin Institute of Technology, the Science and Technology on Advanced Composites in Special Environment Laboratory, State Key Laboratory for Strength and Vibration of Mechanical Structures (SV2017-KF-21) and Young Elite Scientist Sponsorship Program by CAST (YESS20160190).

# Appendix 1. Relative density

The relative density of the pyramidal unit cell with various types of cross-sections is described in Table A-2. For solid and hollow pyramidal lattice cores,  $A_m$  is the cross-sectional area of the truss member, and the mass of the core M is equivalent  $toM = 4lA_m\rho$ . The mass of the hierarchical pyramidal core can be calculated as  $M = 4l(A_m\rho + A_f\rho_f)$  where  $A_f$  is the cross-sectional area of foam-core.

# Appendix 2. The equivalent out-of-plane compressive stiffness of the uniform section lattice trusses

According to the definition of the out-of-plane compressive stiffness and non-dimensional parameter, the compressive stiffness and non-dimensional parameters of sandwich panels with three different cross-sectional shapes are derived in Table A-3. The relevant geometrical dimensions of various types of cross-sections are shown in Fig. 3, and the corresponding abbreviation for parameters in Table A-3 can be expressed as:

$$\begin{split} f(b,b_1,h,h_1) &= (bh-b_1h_1)l^2 \sin^2 \omega + \left(bh^3 - b_1h_1^3\right) \cos^2 \omega \\ f(R,r) &= l^2 \sin^2 \omega \left(R^2 - r^2\right) + 3\left(R^4 - r^4\right) \cos^2 \omega \\ f(a,a_1) &= 2l^2\left(a^2 - a_1^2\right) \sin^2 \omega + \left(a^4 - a_1^4\right) \cos^2 \omega \\ f(b_i,h_i) &= (b_4h_4 - b_3h_3 + b_2h_2 - b_1h_1)l^2 \sin^2 \omega + \left(b_4h_4^3 - b_3h_3^3 + b_2h_3^3 - b_1h_3^3\right) \cos^2 \omega \\ f(r_1,r_2,r_3,r_4) &= \left(r_4^2 - r_3^2 + r_2^2 - r_1^2\right)l^2 \sin^2 \omega + 3\left(r_4^4 - r_3^4 + r_2^4 - r_1^4\right) \cos^2 \omega \\ f(a_1,a_2,a_3,a_4) &= 2l^2\left(a_4^2 - a_3^2 + a_2^2 - a_1^2\right) \sin^2 \omega + \left(a_4^4 - a_3^4 + a_2^4 - a_1^4\right) \cos^2 \omega \end{split}$$

#### Appendix 3. The equivalent out-of-plane compressive property

# 3.1. The external force of each pyramidal lattice truss

Under the out-of-plane compressive loading F along the y-axis, as the pyramidal unit cell is symmetrical, the force along each lattice strut is the same, so the force analysis is performed on any single strut. The vertical downward small displacement  $\delta$  is generated by the external force F. The axial and tangent displacement components along the single strut are  $\delta_A = \delta \sin \omega$  and  $\delta_S = \delta \cos \omega$  respectively. The axial displacement component  $\delta_A$  is generated by the axial force  $F_A$ , and the tangent displacement component  $\delta_S$  is produced by the tangent force  $F_S$  and bending moment  $F_S$ . The corresponding external force components can be obtained by means of the basic mechanics of materials formulas as:

$$F_{A} = \frac{(EA)_{e}}{l}\delta\cos\omega\tag{A-2}$$

$$F_{\rm S} = \frac{12(EI)_e}{l^3} \delta \sin \omega \tag{A-3}$$

$$M = \frac{6(EI)_e}{l^2} \delta \sin \omega \tag{A-4}$$

The total external force F is calculated by  $F = F_A \sin \omega + F_S \cos \omega$ .

# 3.2. The equivalent out-of-plane compressive stiffness

### 3.2.1. The lateral compressive load on a quarter of a unit cell

From the schematic of the pyramidal unit cell in Fig. 2, the symmetrical load F is applied to the y-axis of the unit cell sandwich structure. Due to the symmetry of the structure, the displacement on the mid-section of the unit cell is zero. Assuming that the left and right sides of the unit cell have small displacement  $\delta$ , a quarter of a unit cell is considered as the force analysis object. Fig. 4(a) shows the free-body-diagram of the unit cell under in-plane compression. Under the premise of small deformation, it is considered that the contribution of axial deformation caused by the axial force and tangential deformation caused by the shear and bending moment contribute to the small deformation  $\delta$ . The force-displacement relationship then can be obtained using the deformation compatibility considerations and equilibrium formulation of the partial unit

The axial and tangential displacement components of the truss member can be obtained on the basis of the geometrical relationship where their corresponding expressions are  $\delta_A = \delta \cos \beta$  and  $\delta_S = \delta \sin \beta$ , respectively. The axial displacement  $\delta_A$  is generated by the axial force  $F_A$  and the tangential displacement component  $\delta_S$  is induced by the shear force  $F_S$  and the bending moment M. The boundary conditions at both ends of the truss member are assumed to be clamped. The corresponding expression of the axial force, shear force and bending moment of a single truss can be obtained by means of the basic mechanics of materials formulas and the boundary condition of the lattice truss as:

$$F_{A} = \frac{(EA)_{e}}{l}\delta\cos\beta \tag{A-5}$$

$$F_{S} = \frac{12(EI)_{e}}{I^{3}}\delta\sin\beta \tag{A-6}$$

$$M = \frac{6(EI)_e}{I^2} \delta \sin \beta \tag{A-7}$$

The external force on face sheet of the partial unit cell  $F_f$  which induces the existed small displacement  $\delta$  can be obtained as:

$$F_f = \frac{(EA)_f}{2l\cos\beta}\delta\tag{A-8}$$

where  $(EA)_f$  denotes the equivalent compressive stiffness of the face sheet of the unit cell.

The end force of the bottom face sheet  $F_d$  can be obtained according to the force equilibrium equations as follows.

$$F_d = F_A \cos \beta + F_S \sin \beta + F_f \tag{A-9}$$

Substituting Eqs. (A-5), (A-6) and (A-8) into Eq. (A-9), the end force can be further simplified as:

$$F_d = \left(\frac{(EA)_e l^2 \cos^2 \beta + 12(EI)_e \sin^2 \beta}{l^3} + \frac{(EA)_f}{2l \cos \beta}\right) \delta \tag{A-10}$$

The magnitude of the end force of the top face sheet  $F_u$  equals to that of the external force on face sheet of the partial unit cell  $F_f$ . Moreover, the magnitude of the resultant in-plane compressive force of the unit cell is twice the sum of the end force of the both face sheets and can be expressed as:

$$F = 2F_u + 2F_d \tag{A-11}$$

Substituting Eqs. (A-8) and (A-10) into Eq. (A-11), the resultant force can be further simplified as:

$$F = \frac{2(EA)_f}{l\cos\beta}\delta + \frac{2(EA)_e l^2 \cos^2\beta + 24(EI)_e \sin^2\beta}{l^3}\delta$$
(A-12)

In Eq. (A-12), the first term indicates the external force  $F_f$  on the face sheets, and the second term denotes the external force  $F_c$  on the two truss members. The ratio of  $F_c$  and  $F_f$  is defined as  $\xi_p$  and this non-dimensional parameter is

$$\xi_p = \frac{\pi r_c^2 l_c^2 \cos^2 \beta + 2\pi r_c^4 \sin^2 \beta}{2 l_c^3 t_f}$$
 (A-13)

The axial force of a partial unit cell  $F_A$  is

$$F_A = (1 + \xi_p)F_f \tag{A-14}$$

From the above analysis, the proportion of the load on the  $2^{nd}$  order pyramidal lattice truss will change with the geometric dimensions under in-plane compression. The magnitude of the external force  $F_c$  will reach the collapse strength of the parent material resulting the failure mode on the  $2^{nd}$  order truss.

# 3.2.2. The bending load on a quarter of a unit cell

In order to obtain the equivalent flexural rigidity of the unit cell, the bending moment M is applied to the lateral surface of the hierarchical pyramidal unit cell. Due to the structural symmetry, the displacement and rotation angle of the midsections in the unit cell is zero. The slight rotation angle  $\theta$  induced by the bending moment acts on the side of the structure. In this analysis, a quarter of the hierarchical pyramidal unit cell is considered as a force analysis object. Under the premise of small deformations, the deformation of pyramidal lattice core which has an effect on the bending deformation of the general sandwich structure is also considered. Therefore, both the face sheets and the lattice core will be subjected to the bending moment. According to the deformation compatibility conditions and equilibrium formulation, the free-body diagram of a quarter of a unit cell under bending moment is shown in Fig. 4(b). For the condition, at which one end of the structure is fixed and the other is subjected to a bending moment, the displacement and rotation angle on the free end of the sandwich panels can be derived by means of the mechanics of materials as:

$$\delta = \frac{1}{2}\theta I \cos \beta \tag{A-15}$$

According to the geometric relationship between the vertical, axial and tangential displacement components of the truss, the axial and tangential displacements can be expressed as  $\delta_A = \delta \cos\theta$  and  $\delta_S = \delta \sin\theta$ , respectively. The axial force can be derived from the mechanics of materials and be expressed as:

$$F_{A} = \frac{1}{2} (EA)_{e} \theta \cos \theta \cos \beta \tag{A-16}$$

The tangential displacement  $\delta_S$  is induced by the shear force  $F_S$  and bending moment M which are applied to the end of the truss. From the basic mechanics of materials formulas, the tangential displacement is:

$$\delta_{S} = \frac{M_{c}l^{2}}{2(EI)_{\rho}} - \frac{F_{S}l^{3}}{3(EI)_{\rho}}$$
(A-17)

Based on the continuous displacements, the rotation angle  $\theta$  of the truss end is equal to that of the face sheet. The rotation angle of the truss end which is induced by both the shear force  $F_S$  and the bending moment  $M_c$ . With the aid of basic mechanics of materials formulas, the rotation angle is:

$$\theta = \frac{M_c l}{(EI)_e} - \frac{F_s l^2}{2(EI)_e} \tag{A-18}$$

By combination of the expression of the tangential displacement component of the truss and Eqs. (A-17), (A-18), the expression for the shear force and the bending moment can be obtained as:

$$F_{\rm S} = \frac{6(EI)_e}{I^2} (1 - \cos\beta \sin\theta)\theta \tag{A-19}$$

$$M_c = \frac{(EI)_e}{I} (4 - 3\cos\beta\sin\theta)\theta \tag{A-20}$$

The shear force of face sheets which is induced by the lattice core is defined as  $F_{cs}$ . Using the equilibrium equations, the shear force can be presented as:

$$F_{\rm CS} = F_{\rm A}\cos\theta - F_{\rm S}\sin\theta \tag{A-21}$$

Substituting Eqs. (A-16), (A-19) into Eq. (A-21), the shear force can be further simplified as:

$$F_{cs} = \frac{1}{2} (EA)_e \theta \cos \beta \cos^2 \theta - \frac{6(EI)_e}{I^2} \theta \left( \sin \theta - \cos \beta \sin^2 \theta \right)$$
 (A-22)

From the force relationship, the rotation angle  $\theta$  is determined by the shear force  $F_{cs}$  of the lattice core, the bending moment  $M_c$  on the truss rod and external bending moment  $M_d$ . According to the basic mechanics of materials formulas, the corresponding expression of the rotation angle is:

$$\theta = \frac{2M_d l \cos \beta}{(EI)_m} - \frac{2M_c l \cos \beta}{(EI)_m} + \frac{F_{cs} l^2 \cos^2 \beta}{(EI)_m}$$
(A-23)

where  $(EI)_m$  is the flexural rigidity of the face sheet relative to the neutral layer.

Substituting Eqs. (A-20), (A-22) into Eq. (A-23), the external bending moment can be simplified as:

$$M_d = \frac{(EI)_m}{2l\cos\beta}\theta + \left[f_1(\beta,\theta)\frac{(EI)_e}{l} + f_2(\beta,\theta)l(EA)_e\right]\theta \tag{A-24}$$

where  $f_1(\beta, \theta)$  and  $f_2(\beta, \theta)$  are expressed as  $4 - 6\cos\beta\sin\theta + 3\cos^2\beta\sin^2\theta$  and  $\frac{1}{4}\cos^2\beta\cos^2\theta$ , respectively. In Eq. (A-24), the first term represents the contribution of the bottom face sheet to the bending moment, and the second term is the contribution of the lattice core to the bending moment.

The bending moment  $M_u$  needs to be applied when the rotation angle  $\theta$  is generated at the end of the upper panel. Based on the basic mechanics of materials formulas, the bending moment  $M_u$  is

$$M_u = \frac{(EI)_m}{2I\cos\beta}\theta\tag{A-25}$$

The external applied total bending moment is twice the sum of the bending moments  $M_d$  and  $M_u$ , namely,  $M = 2M_d + 2M_u$ . Substituting Eqs. (A-24) and (A-25) into this expression, the total bending moment can be further expressed as:

$$M = \frac{2(EI)_m}{l\cos\beta}\theta + \left[f_1(\beta,\theta)\frac{(EI)_e}{l} + f_2(\beta,\theta)l(EA)_e\right]\theta \tag{A-26}$$

where  $(EI)_m = Eb_c t_f^3/12 + (l_c \sin \omega + t_f)^2 Eb_c t_f/4$  and the equivalent flexural rigidity of the unit cell  $(EI)_e$  is  $(EI)_e = 2Ml_c \cos \beta/\theta$ .

# 3.2.3. The equivalent out-of-plane compressive strength

3.2.3.1. The shear load on a quarter of a unit cell. The in-plane shear load F is applied on a pyramidal unit cell along the x-axis, shown in Fig. 4(c). The derivation process of this unit cell under shear load is similar to the method in Section 3.1 of Appendix 3. The corresponding axial force  $F_A$  and external shear load F can be respectively expressed as:

$$F_{A} = \frac{(EA)_{e}}{l}\delta\cos\alpha\tag{A-27}$$

$$F = \frac{4(EA)_e I^2 \cos^2 \alpha + 48(EI)_e \sin^2 \alpha}{I^3} \delta$$
 (A-28)

where the non-dimensional parameter  $\xi_{\alpha}$  can be expressed as:

$$\xi_{\alpha} = \frac{(EA)_{e} l^{2} \cos^{2} \alpha + 12(EI)_{e} \sin^{2} \alpha}{(EA)_{e} l^{2} \cos \alpha}$$
(A-29)

Therefore, the relationship between the external shear load and axial force is shown in Eq. (13).

3.2.3.2. The uniform section lattice trusses. The pyramidal lattice trusses with uniform sections include solid, hollow and foam-core sandwich struts with different cross-section shapes. Sandwich structures with solid/hollow lattice trusses belong to non-hierarchical structures. However, the sandwich structures with foam-core lattice trusses are typical kinds of hierarchical structures. The two dominant failure modes of the pyramidal lattice truss that occur with an increase in the out-of-plane compressive loads include core member buckling of the pyramidal lattice truss and core member crushing of the pyramidal lattice core.

The critical Euler buckling load of the truss in the case of core member buckling of the pyramidal lattice truss (Hearn, 1997) can be written as:

$$F_{A} = \frac{\pi^{2} (EI)_{e}}{\mu^{2} l^{2}} \tag{A-30}$$

where  $F_A$  and  $(El)_e$  respectively represent the axial force and the equivalent flexural rigidity of the lattice truss. l is the length of the lattice truss. The parameter  $\mu$  is assumed to be equal to 0.5 considering both ends of the strut to be clamped. Substituting Eq. (A-30) into Eqs. (13) and (16), the closed-form expression of equivalent out-of-plane compressive strength of the unit cell can be obtained as:

$$\bar{\sigma} = \frac{8\xi_{\omega}\pi^2(EI)_e}{l^4\cos^2\omega} \tag{A-31}$$

In the case of core member crushing of the pyramidal lattice core, the failure mode is characterized by crushing of the lattice truss members. In this study, the mechanical properties of carbon-epoxy are used for establishing the material model in the numerical analysis. The elastic modulus and compressive strength of the parent material are 100 GPa and 800 MPa, respectively. The axial force of the lattice truss can be expressed as:

$$F_A = \sigma_f A_m \tag{A-32}$$

where the corresponding strength at which the crushing failure of the parent material occurs is  $\sigma_f$  and the cross-sectional area of the lattice truss is  $A_m$ . Substituting Eq. (A-32) into Eqs. (13) and (16), the equivalent out-of-plane compressive strength can be further simplified as:

$$\bar{\sigma} = \frac{2\xi_{\omega}\sigma_f A_m}{l^2 \cos^2 \omega} \tag{A-33}$$

Substituting the equivalent flexural rigidity (EI)<sub>e</sub> of pyramidal truss members and the dimensionless parameter  $\xi_{\omega}$  of pyramidal lattice trusses with various sectional configurations into Eqs. (A-31) and (A-33), the corresponding equivalent out-of-plane compressive strength of pyramidal unit cell under two failure modes can be obtained. Table 1 lists the compressive strength of pyramidal sandwich panels with three cross-sectional properties which include the solid, hollow and foam-core truss members and each cross-sectional property consists of three cross-section shapes (i.e. rectangle, circle and equilateral triangle).

# 3.3. Comparative out-of-plane compressive properties

# 3.3.1. Stiffness of the uniform cross-sectional lattice trusses

The out-of-plane compressive stiffness of pyramidal sandwich structure with various truss members of various cross sections can be expressed succinctly as

$$\bar{E} = \frac{\sqrt{2}\xi_{\omega}E}{4}\bar{\rho} \tag{A-34}$$

where the parameter  $\overline{\rho}$  denotes the relative density of the 1<sup>st</sup> order pyramidal unit cell and the corresponding expression has been defined in Table 3.

In Eq. (A-34), the dimensionless parameter  $\xi_\omega$  is the shape factor, whose expressions for various solid and hollow cross-sectional lattice struts with arbitrary sectional shape is listed in Table A-3. These expressions typically contain a leading angular sine term which is same for all cross sections and an additional cross section dependent function. For the stretch dominated lattice cores, the cross-sectional dimensions of struts are much smaller than the length of the truss members which diminishes the magnitude of second function making  $\xi_\omega \approx \sin\omega$ . This suggests that the out-of-plane compressive stiffness of the pyramidal sandwich panels with various lattice truss cross sections are nearly equal for similar relative density.

# 3.3.2. Strength of the uniform cross-sectional lattice trusses

3.3.2.1. Core member buckling of the pyramidal lattice trusses. For the pyramidal lattice struts with circular section, equivalent out-of-plane strength of pyramidal lattice structure with core member buckling is expressed as a function of relative density. The relative density itself depends on the geometry of the structural members. For hollow circular cross sections, the inner (r) and outer radii (R) can be related using a proportional factor  $g_h$  leading to  $r = g_h R$ . The geometry of the foam core consists of several concentric circles of radii  $r_i$  which can be related sequentially with proportionality constants  $g_f$  leading to the set  $r_i = g_f r_{i+1}$ . These non-dimensional constants are useful in expressing equivalent compressive strengths of struts of similar lengths and cross sections. This can be achieved by defining the non-dimensional factors  $f_h$  and  $f_m$ . Here  $f_h$  is defined as a function of the proportional factor  $g_f$ . Substituting the corresponding parameters of circular section which include the dimensionless diameter  $\xi_\omega$  (Table A-3) and the relative density of the pyramidal unit cell (Table A-2) into the equivalent buckling strength of the pyramidal unit cell with circular section (Table 1), these expressions come out to be (see Table 3):

$$f_h(g_h) = (1 + g_h^2)/(1 - g_h^2) f_m(g_f) = (1 - g_f^4 + g_f^8 - g_f^{12})/(1 - g_f^2 + g_f^4 - g_f^6)^2$$
(A-35)

From the three formulas in Table 3, the structural functions  $f_h(g_h)$  and  $f_m(g_f)$  determine the buckling resistance of the circular sectional struts. To ensure the same relative density, the cross-sectional area of the struts with hollow and foamcore sections need to be consistent.

$$\pi R^2 (1 - g_h^2) = \pi r_4^2 (1 - g_f^2 + g_f^4 - g_f^6) \tag{A-36}$$

Then, in order to establish the connection between the wall thickness of two lattice trusses, the wall thickness of the hollow section is *x* times the thickness of outer wall of the foam-core pyramidal struts

$$R(1 - g_h) = xr_4(1 - g_f) \tag{A-37}$$

Substituting Eq. (A-37) into Eq. (A-36), the buckling strength coefficient  $f_h(g_h)$  can be obtained

$$f_h(g_h) = \frac{1 - g_f^2 + g_f^4 - g_f^6}{2x^2(1 - g_f)^2} + \frac{x^2(1 - g_f)^2}{2(1 - g_f^2 + g_f^4 - g_f^6)}$$
(A-38)

The two buckling strength coefficients  $f_h(g_h)$  and  $f_m(g_f)$  versus the proportional coefficient  $g_f$  are shown in Fig. 9(a). For a case where the thickness of hollow struts is two times that of foam hollow sandwich strut, the critical buckling load of the foam hollow sandwich is greater than that of the hollow struts. The buckling capacity is shown to be a function of the ratio  $g_f$ . Here, some case-study parameters are taken as an example to investigate the relationship between the sectional geometric parameters and buckling resistance of the lattice struts. The out-of-plane compressive strength versus relative density curve is shown in Fig. 9(b) for x = 2 and  $g_f = 0.8$ . Similar procedure can be used for non-circular cross sections. The out-of-plane compressive strength of triangular section truss members versus relative density curve is shown in Fig. 9(c) for x = 3 and  $g_f = 0.8$ . Due to the different aspect ratio of rectangular section, the two buckling strength coefficients of the rectangular section lattice struts cannot be represented by a single parameter and the mechanical properties of rectangular sections are usually simplified to square sections (Ashby, 2005). The parametric form of the buckling strength of the rectangular section lattice struts are same with those of circular section truss members. Fig. 9(d) shows the out-of-plane compressive strength of sandwich structures with rectangular section lattice struts versus relative density curve when x = 2 and  $g_f = 0.7$ .

3.3.2.2. Core member crushing of the pyramidal lattice trusses. The out-of-plane compressive strength of the pyramidal lattice structure with various cross-sections can be expressed as a function of relative density (by substituting the relative density in Table A-2 into the equivalent crushing strength of the lattice truss in Table 1)

$$\overline{\sigma} = \frac{\xi_{\omega} \sigma_{f}}{\sqrt{2}} \overline{\rho} \tag{A-39}$$

This expression is similar to the equivalent out-of-plane compressive stiffness in Eq. (A-34). When the core member crushing failure mode occurs, the corresponding equivalent out-of-plane compressive strength is almost unaffected by the cross-section of the lattice truss.

Fig. 9(a)–(c) show that the buckling failure mode of lattice struts with various cross-sections are in the lower relative density area. However, the core member crushing occurs in the higher relative density area. This is because for the core member buckling failure mode, the equivalent out-of-plane compressive strength of sandwich panels of lattice struts with various cross-sections is in a quadratic relationship with the relative density. For the core member crushing, the compressive strength of pyramidal lattice sandwich panels with various sectional properties scale linearly to relative density. For a cross-section with the same shape, the critical relative density corresponding to the intersection of buckling and crushing is the highest for the sandwich panels with solid section lattice truss and the buckling resistance of the solid lattice core is the weakest. However, for the hollow lattice truss, as its second moment of area increases, the corresponding flexural rigidity and the buckling resistance of the hollow lattice struts increase as well. For the foam-core sandwich struts, the buckling resistance is related to the wall thickness and the proportionality coefficient  $g_f$  of the inner and outer walls where the wall

thickness has the greatest effect among the other factors. When the outer-wall thickness of foam-core sandwich truss is less than one half of the wall thickness of the hollow structure, the advantages of the foam-core sandwich structure in buckling resistance can be shown for any coefficient of proportionality. When the outer wall thickness of the foam-core sandwich truss is greater than two-thirds of the wall thickness of the hollow truss, the buckling resistance of the foam-core sandwich truss is less than that of the hollow truss because of the smaller relative moment of inertia of the foam-core sandwich truss compared to the hollow truss with the same relative density.

#### Appendix 4. The equivalent shear property

4.1. The equivalent shear stiffness of the uniform cross-sectional lattice trusses

The uniform cross-section lattice trusses consist of solid, hollow and foam-core sandwich struts with three cross-sectional shapes. The corresponding expressions of the equivalent compressive stiffness and equivalent flexural rigidity of truss members with various cross-sectional shapes are derived in Table A-4. Substituting the equivalent compressive stiffness  $(EA)_e$ and the equivalent flexural rigidity  $(EI)_e$  of lattice trusses with various sectional configurations into Eqs. (26) and (29), the dimensionless parameter  $\xi_{\alpha}$  and the shear stiffness of the unit cell G for pyramidal struts with different cross-sectional shapes are listed in Table 4. For the sake of brevity, the dimensionless parameter  $\xi_{\alpha}$  in the expression of the shear stiffness is not further expanded (Table 5).

# 4.2. The equivalent shear strength

4.2.1. The pyramidal-pyramidal hierarchical lattice trusses

4.2.1.1. Face sheet wrinkling (FW) of the  $2^{nd}$  order lattice trusses. According to the basic mechanics of materials formulas, the critical force of the face sheets is

$$F_f = \frac{\pi^2 (EI)_e}{2\mu^2 l_c^2 \cos^2 \beta} \tag{A-40}$$

where the parameter is  $\mu = 0.5$ , and the equivalent flexural rigidity of the face sheets is  $(EI)_e = Ebt_f^3/12$ . Substituting Eq. (A-15) into Eq. (A-11), the axial force of the partial unit cell is

$$F_{A} = \frac{(1 + \zeta_{p})\pi^{2}Ebt_{f}^{3}}{6l_{c}^{2}\cos^{2}\beta}$$
 (A-41)

4.2.1.2. Face sheet crushing (FC) of the  $2^{nd}$  order lattice trusses. The crushing strength of the face sheets is  $\sigma_f$ , and the corresponding external force of the face sheets is Eq. (24). Substituting Eq. (24) into Eq. (A-11), the axial force of the partial unit cell is

$$F_A = (1 + \zeta_p)2bt_f\sigma_f \tag{A-42}$$

4.2.2. The uniform cross-sectional of lattice trusses

Here, the failure modes of the unit cell under shear loads are similar to those under the out-of-plane compressive loads in Section 3.5.2. There will be two failure modes in the pyramidal sandwich structures under shear load: (1) core member buckling of the pyramidal lattice core; (2) core member crushing of the pyramidal lattice truss.

4.2.2.1. Core member buckling of the pyramidal lattice trusses. Substituting the buckling critical load of struts described in Table 2 into Eq. (33), the equivalent out-of-plane shear strength of the pyramidal unit cell can be expressed as:

$$\overline{\tau} = \frac{8\xi_{\alpha}\pi^{2}(EI)_{e}}{l^{4}(\sin\varphi + \cos\varphi)\cos^{2}\omega}$$
(A-43)

4.2.2.2. Core member crushing of the pyramidal lattice trusses. The crushing strength of the parent material which is composed of the sandwich panels is defined as  $\sigma_f$ , and  $A_m$  is the cross-sectional area of the truss member. The axial force corresponding to the collapse of the strut in the truss members is

$$F_A = \sigma_f A_m \tag{A-44}$$

Substituting Eq. (A-44) into Eq. (33), the equivalent shear strength of the unit cell is

$$\bar{\tau} = \frac{2\xi_{\alpha}\sigma_f A_m}{l^2(\sin\varphi + \cos\varphi)\cos^2\omega} \tag{A-45}$$

The equivalent flexural rigidity (EI)<sub>e</sub> and the dimensionless parameter  $\xi_{\alpha}$  are the only two variables in the expression of the equivalent shear strength of the pyramidal unit cell under buckling and crushing failure modes. Therefore, the equivalent shear strength of pyramidal sandwich structures with various uniform cross-sectional shapes can be deduced by substituting corresponding expressions as listed in Table A-4 and Table 4.

 Table A-1

 The specification of the specimens used for compressive property simulations (mm).

Relative density $\overline{\rho}(\%)$	Structural topologies	Truss I $(l \times b_f \times t_f)$	Truss II $(l_c \times r_c)$
0.102	1 <sup>st</sup> order	62.91 × 2.49 × 0.236	
	2 <sup>nd</sup> order	$62.91 \times 2.49 \times 0.1$	$1.33 \times 0.0578$
0.122	1 <sup>st</sup> order	$72.48\times2.87\times0.326$	1
	2 <sup>nd</sup> order	$72.48\times2.87\times0.14$	$1.50\times0.071$
0.133	1 <sup>st</sup> order	$103.3\times4.09\times0.506$	1
	2 <sup>nd</sup> order	$103.3\times4.09\times0.21$	$2 \times 0.12$
0.166	1 <sup>st</sup> order	$72.48\times4.30\times0.326$	1
	2 <sup>nd</sup> order	$72.48\times4.30\times0.14$	$1.5\times0.071$
0.221	1 <sup>st</sup> order	$103.3\times8.18\times0.506$	1
	2 <sup>nd</sup> order	$103.3\times8.18\times0.21$	2 × 0.12

**Table A-2**The relative density of the pyramidal unit cell with various types of cross-sections.

Sectional properties-relative densities $(\overline{ ho})$				
Solid/hollow $\frac{2A_m}{l^2\cos^2\omega\sin\omega}$	Foam core $\frac{2(A_m + A_f \rho_f / \rho)}{l^2 \cos^2 \omega \sin \omega}$	Rectangle $\frac{2bh}{l^2\cos^2\omega\sin\omega}$	Circle $\frac{2\pi R^2}{l^2 \cos^2 \omega \sin \omega}$	Regular triangle $\frac{\sqrt{3}a^2}{2l^2\cos^2\omega\sin\omega}$

**Table A-3**The equivalent compressive stiffness of the pyramidal unit cell with various types of cross-sections.

Sectional properties	Dimensionless parameter $(\xi_{\omega})$	Equivalent compressive stiffness $(\overline{E}/\text{MPa})$
Solid rectangle	$\sin \omega + \frac{h^2 \cos^2 \omega}{l^2 \sin \omega}$	$\frac{2\xi_{\omega}Ebhsin^2\omega}{l^2cos^2\omega}$
Hollow rectangle	$\sin \omega + \frac{(bh^3 - b_1h_1^3)\cos^2\omega}{(bh - b_1h_1)l^2\sin\omega}$	$\frac{2f(b,b_1,h,h_1)E\sin\omega}{l^4\cos^2\omega}$
Foam rectangle	$\sin \omega + \frac{(b_4 h_4^3 - b_3 h_3^3 + b_2 h_3^3 - b_1 h_3^3)\cos^2 \omega}{(b_4 h_4 - b_3 h_3 + b_2 h_2 - b_1 h_1)l^2 \sin \omega}$	$\frac{2Ef(b_i,h_i)\sin\omega}{l^4\cos^2\omega}$
Solid circle	$\sin \omega + \frac{3R^2\cos^2\omega}{l^2\sin\omega}$	$\frac{2\pi\xi_{\omega}ER^2\sin^2\omega}{l^2\cos^2\omega}$
Hollow circle	$\sin \omega + \frac{3(R^2+r^2)\cos^2\omega}{l^2\sin\omega}$	$\frac{2\pi Ef(R,r)\sin\omega}{l^4\cos^2\omega}$
Foam circle	$\sin \omega + \frac{3(r_4^4 - r_3^4 + r_2^4 - r_1^4)\cos^2 \omega}{(r_4^2 - r_3^2 + r_2^2 - r_1^2)l^2\sin \omega}$	$\frac{2Ef(r_1,r_2,r_3,r_4)\pi\sin\omega}{I^4\cos^2\omega}$
Solid triangle	$\sin \omega + \frac{a^2 \cos^2 \omega}{2l^2 \sin \omega}$	$\frac{\sqrt{3}\xi_{\omega}Ea^{2}\sin^{2}\omega}{2l^{2}\cos^{2}\omega}$
Hollow triangle	$\sin \omega + \frac{(a^2+a_1^2)\cos^2\omega}{2l^2\sin\omega}$	$\frac{\sqrt{3}f(a,a_1)E\sin\omega}{4l^4\cos^2\omega}$
Foam triangle	$\sin \omega + \frac{(b_4 h_4^3 - b_3 h_3^3 + b_2 h_3^3 - b_1 h_3^3)\cos^2 \omega}{(b_4 h_4 - b_3 h_3 + b_2 h_2 - b_1 h_1)l^2 \sin \omega}$	$\frac{\sqrt{3}\text{Ef}(a_1, a_2, a_3, a_4) \sin \omega}{4l^4 \cos^2 \omega}$

**Table A-4**The equivalent compressive stiffness and equivalent flexural rigidity of the lattice strut with various types of cross-sections.

Sectional properties	Equivalent compressive stiffness (EA) <sub>e</sub>	Equivalent flexural rigidity (EI)e
Solid rectangle	Ebh	Ebh <sup>3</sup> /12
Hollow rectangle	$E(bh-b_1h_1)$	$E(bh^3 - b_1h_1^3)/12$
Foam rectangle	$E(b_4h_4-b_3h_3+b_2h_2-b_1h_1)$	$E(b_4h_4^3-b_3h_3^3+b_2h_2^3-b_1h_1^3)/12$
Solid circle	$E\pi R^2$	$E\pi R^4/4$
Hollow circle	$E\pi\left(R^2-r^2\right)$	$E\pi (R^4 - r^4)/4$
Foam circle	$E\pi \left( r_4^2 - r_3^2 + r_2^2 - r_1^2 \right)$	$E\pi (r_4^4 - r_3^4 + r_2^4 - r_1^4)/4$
Solid triangle	$\sqrt{3}Ea^2/4$	$\sqrt{3}Ea^4/96$
Hollow triangle	$\sqrt{3}E(a^2-a_1^2)/4$	$\sqrt{3}E(a^4-a_1^4)/96$
Foam triangle	$\sqrt{3}E(a_4^2-a_3^2+a_2^2-a_1^2)/4$	$\sqrt{3}E(a_4^4-a_3^4+a_2^4-a_1^4)/96$

# 4.3. Comparative shear properties

# 4.3.1. Stiffness of the uniform cross-sectional lattice trusses

The equivalent shear stiffness of pyramidal lattice sandwich structure with the uniform cross-section can be expressed as a function of relative density, and the corresponding unified expression is

$$\overline{G} = \xi_{\alpha} E \cos \alpha \sin^2 \omega \bar{\rho} \tag{A-46}$$

where the dimensionless parameter  $\xi_{\alpha}$  in Eq. (A-46) under different conditions has been given in Table 4. Due to the fact that the ratio of the length to diameter of the truss members is larger, the dimensionless parameter of various sectional types is almost the same.

4.3.2. Strength of the uniform cross-sectional lattice trusses

4.3.2.1. Core member crushing of the pyramidal lattice trusses. The relationship between the equivalent shear strength of various types of sandwich structures and relative density has the following form

$$\frac{\bar{\tau}_{zy}}{\sigma_f \bar{\rho}} + \frac{\bar{\tau}_{zx}}{\sigma_f \bar{\rho}} = \xi_\alpha \sin \omega \tag{A-47}$$

Since the equivalent shear strength varies with the angle  $\varphi$  between the external load and the x-axis, the curve which shows equivalent shear strength versus relative density cannot describe the shear strength of pyramidal sandwich unit cell completely. In Eq. (A-47), if the first term represents loading along y-axis, and the second term along x-axis, then the corresponding failure envelop curve is shown in Fig. 13(a). This figure describes that the distance between the points of failure envelop curve and initial point equals the magnitude of shear strength. The angle between the x-axis and the connecting line of these two points is defined as  $\varphi$ . In addition, the equivalent shear strength changes periodically with the angle with period  $\pi/2$ , which is consistent with the periodicity of the pyramidal sandwich structure. When  $\varphi$  satisfies  $\varphi = k\pi/2$  (k belonging to a natural number), the magnitude of shear strength is maximum. Moreover, the angle satisfies  $\varphi = (2k+1)\pi/4$ (k is a natural number), and the corresponding magnitude of the equivalent shear strength is minimum.

4.3.2.2. Core member buckling of the pyramidal lattice trusses. For pyramidal lattice truss members with the rectangular solid cross-sectional property, the ratio of length to width satisfies the equation h = fb. The failure equation is therefore,

$$\frac{\bar{\tau}_{zy}}{E\bar{\rho}^2} + \frac{\bar{\tau}_{zx}}{E\bar{\rho}^2} = \frac{1}{24}\xi_\alpha \pi^2 f \tag{A-48}$$

For the rectangular hollow section struts, the inner and outer wall thickness satisfies:  $h_1 = f_h b_1$ ,  $h_1 = f_h b$ ,  $h_1 = f_h b$ . The corresponding failure equation is obtained as:

$$\frac{\bar{\tau}_{zy}}{E\bar{\rho}^2} + \frac{\bar{\tau}_{zx}}{E\bar{\rho}^2} = \frac{1}{24}\xi_\alpha \pi^2 f(f_h) \tag{A-49}$$

where the parameter in Eq. (A-49) is  $f(f_h) = f_h(1 + f_h^2)/(1 - f_h^2)$ .

For the rectangular foam-core sandwich struts, the geometric parameters satisfies:  $b_i = f_f b_{i+1}$ ,  $h_i = f_f h_{i+1}$ ,  $h_i = f_f b_i$  (i = 1, 2, 3...) leading to,

$$\frac{\bar{\tau}_{zy}}{E\bar{\rho}^2} + \frac{\bar{\tau}_{zx}}{E\bar{\rho}^2} = \frac{1}{24} \xi_{\alpha} \pi^2 f(f_{\rm f}) \tag{A-50}$$

where the parameter in Eq. (A-50) is  $f(f_f) = f_{\rm f}(1-f_{\rm f}^4+f_{\rm f}^8-f_{\rm f}^{12})/(1-f_{\rm f}^2+f_{\rm f}^4-f_{\rm f}^6)^2$ . The structural function of the rectangular section is related to the ratio of length to width. To simplify the connection between structural functions  $f(f_h)$  and  $f(f_f)$  a quadrate section is adopted to substitute the rectangular section, and to ensure that the relative density of various structural forms remains the same. The wall thickness of hollow struts is x times than that of the foam-core sandwich struts. For x = 2,  $f_f = 0.7$ , the failure envelope curve of shear buckling strength is plotted in Fig. 13(b). For a set of parameters is x = 2,  $f_f = 0.8$ , another set of parameters is x = 3,  $f_f = 0.8$ . The corresponding failure envelop curves of shear buckling strength with circular and triangular section properties are also shown in Fig. 13(c) and (d). From this figure, under the same cross-sectional shape of struts, the failure envelop curve of sandwich structures with solid truss members encloses the smallest area. Thus, this type of lattice struts has the weakest anti-buckling property. Meanwhile, for a given mass, the sandwich structure with foam-core lattice truss has stronger ability to resist buckling.

# References

Ajdari, A., Nayeb-Hashemi, H., Vaziri, A., 2011. Dynamic crushing and energy absorption of regular, irregular and functionally graded cellular structures. Int. J. Solids Struct. 48 (3), 506-516.

Ashby, M., 2005. Hybrids to fill holes in material property space. Philos. Mag. 85 (26-27), 3235-3257.

Biagi, R., Bart-Smith, H., 2012. In-plane column response of metallic corrugated core sandwich panels. Int. J. Solids Struct. 49 (26), 3901-3914.

Coelho, P., Rodrigues, H., 2015. Hierarchical topology optimization addressing material design constraints and application to sandwich-type structures. Struct. Multidiscip. Optim. 52 (1), 91-104.

Cote, F., et al., 2009. The through-thickness compressive strength of a composite sandwich panel with a hierarchical square honeycomb sandwich core. J. Appl. Mech. 76 (6), 061004.

Cote, F., et al., 2007. Structural response of pyramidal core sandwich columns. Int. J. Solids Struct. 44 (10), 3533-3556.

Cui, X., et al., 2012. A lattice deformation based model of metallic lattice sandwich plates subjected to impulsive loading. Int. J. Solids Struct. 49 (19),

Dong, L., Wadley, H., 2015. Mechanical properties of carbon fiber composite octet-truss lattice structures. Compos. Sci. Technol. 119, 26-33.

Dharmasena, K., et al., 2011. Response of metallic pyramidal lattice core sandwich panels to high intensity impulsive loading in air. Int. J. Impact Eng. 38 (5), 275-289.

Evans, A., 2001. Lightweight materials and structures. MRS Bull. 26 (10), 790-797.

Fan, H., Jin, F., Fang, D., 2008. Mechanical properties of hierarchical cellular materials. part i: Analysis. Compos. Sci. Technol. 68 (15), 3380-3387.

Fan, H., Fang, D., 2009. Enhancement of mechanical properties of hollow-strut foams: analysis. Mater. Des. 30 (5), 1659-1666.

Feng, L., Wu, L., Yu, G., 2016. An hourglass truss lattice structure and its mechanical performances. Mater. Des. 99, 581-591.

Finnegan, K., et al., 2007. The compressive response of carbon fiber composite pyramidal truss sandwich cores. Int. J. Mater. Res. 98 (12), 1264-1272.

Fleck, N., Deshpande, V., Ashby, M., 2010. Micro-architectured materials: past, present and future. In Proc. R. Soc. A. 466 (2121), 2495–2516.

Haghpanah, B., et al., 2013. Self-similar hierarchical honeycombs. In Proc. R. Soc. A. 469 (2156), 20130022.

Han, S., Lee, J., Kang, K., 2015. A new type of low density material: shellular, Adv. Mater. 27 (37) 5506-5011.

Hearn, E.J., 1997. Mechanics of Materials 2. Butterworth-Heinemann, Linacre House, Jordan Hill, Oxford, pp. 28–60.

He, Z.Z., et al., 2017. Mechanical properties of copper octet-truss nanolattices. J. Mech. Phys. Solids 101, 133-149.

Li, M., et al., 2011. Structural response of all-composite pyramidal truss core sandwich columns in end compression. Compos. Struct. 93 (8), 1964-1972.

Liu, T., Deng, Z., Lu, T., 2007. Minimum weights of pressurized hollow sandwich cylinders with ultralight cellular cores. Int. J. Solids Struct. 44 (10), 3231–3266.

Liu, L., et al., 2017. Elastic and failure response of imperfect three-dimensional metallic lattices: the role of geometric defects induced by Selective Laser Melting. J. Mech. Phys. Solids. 107, 160–184.

Liu, J., et al., 2018. Investigation on manufacturing and mechanical behavior of all-composite sandwich structure with Y-shaped cores. Compos. Sci. Technol. 159, 87–102.

Meza, L.R., et al., 2015. Resilient 3D hierarchical architected metamaterials. Proc. Natl Acad. Sci. U.S.A. 112 (37), 11502-11507.

Vigliotti, A., Pasini, D., 2012. Mechanical properties of hierarchical lattices. Mech. Mater. 62, 32-43.

Wu, Q, et al., 2017. Mechanical properties and failure mechanisms of sandwich panels with ultra-lightweight three-dimensional hierarchical lattice cores. Int. J. Solids Struct.

Xiong, J., et al., 2012a. Shear and bending performance of carbon fiber composite sandwich panels with pyramidal truss cores. Acta Mater. 60 (4), 1455–1466.

Xiong, J., et al., 2012b. Mechanical behavior of carbon fiber composite lattice core sandwich panels fabricated by laser cutting. Acta Mater. 60 (13–14), 5322–5334.

Xiong, I., et al., 2015. Advanced microlattice materials. Adv. Eng. Mater. 17 (9), 1253-1264.

Xu, H., Farag, A., Pasini, D., 2017. Multilevel hierarchy in bi-material lattices with high specific stiffness and unbounded thermal expansion. Acta Mater. 134, 155–166.

Yin, S., Wu, L., Nutt, S., 2013. Stretch-bend-hybrid hierarchical composite pyramidal lattice cores. Compos. Struct. 98, 153-159.

Zhang, Q., et al., 2015. Bioinspired engineering of honeycomb structure using nature to inspire human innovation. Prog. Mater. Sci. 74, 332-400.

Zok, F.W., Latture, R.M., Begley, M.R., 2016. Periodic truss structures. J. Mech. Phys. Solids. 96, 184-203.